TECHNISCHE UNIVERSITÄT WIEN

LINKÖPING UNIVERSITY

DIPLOMARBEIT

Polarizing Multilayer Neutron Mirrors

zur Erlangung des akademischen Grades

Diplom-Ingenieur

im Rahmen des Studiums

Technische Physik

eingereicht von

Martin Wess
Matrikelnummer 01325756

ausgeführt am Atominstitut
der Fakultät für Physik der Technischen Universität Wien
in Zusammenarbeit mit der Universität Linköping

Betreuung
Betreuer: Univ.Prof. Dipl.-Ing. Dr.techn. Gerald Badurek
Mitwirkung: Ass.Prof. Dipl.-Ing. Dr.techn. Erwin Jericha
Mitwirkung: Assoc.Prof. Dr.techn. Fredrik Eriksson (Linköping)

Wien, 01.04.2019

(Unterschrift Verfasser) (Unterschrift Betreuer)

Zusammenfassung

Diese Diplomarbeit beschreibt Prinzip, Design, Herstellung und Charakterisierung von polarisierenden Vielschicht-Neutronenspiegeln. Das Hauptaugenmerk wurde auf die Optimierung der Umgebungsparameter während der Herstellung gelegt, um möglichst ideale Grenzflächen zu generieren. Die Grenzflächen sollen minimale Rauheit und Mischung zwischen den Schichten aufweisen, um Neutronenspiegel mit hoher Qualität zu erhalten.

Um polarisierende Vielschicht-Neutronenspiegel herzustellen, muss eines der beiden gewählten Materialien ferromagnetisch sein. Außerdem ist es wichtig, dass das nukleare Fermi-Pseudopotential für den niedrigeren Spinzustand des ferromagnetischen Partners möglichst gleich groß ist wie das des unmagnetischen Materials. Cobalt (Co) und Titan (Ti) erfüllen diese Voraussetzungen und wurden daher als Materialien gewählt. Der Einfluss der Beimischung von isotopangereichertem, schwach Neutron-absorbierendem Borcarbid ($^{11}B_4C$) auf die Qualität der Grenzflächen wurde gründlich untersucht.

Die Proben wurden mittels ionenunterstützter Gleichstrom - Magnetronsputterkathodenzerstäubung mit zwei unterschiedlichen Depositionssystemen hergestellt. Der Unterschied zwischen kontinuierlicher und modulierter Ionenunterstützung wurde untersucht. Bei zweiterer Methode wird der erste Teil jeder Schicht mit Ionenunterstützung mit niedriger Energie erzeugt, während der zweite Teil Ionen mit höherer Energie verwendet.

Eines der Depositionssysteme bot die Möglichkeit, Proben mithilfe von Ionenunterstützung mit hohem Fluss herzustellen. Dies wurde verwendet, um den Einfluss unterschiedlicher Ionenflüsse auf die Qualität der vielschichtigen Strukturen zu testen.

Die Proben wurden in erster Linie durch Röntgenreflektometrie (XRR) und diffuse Röntgenstreuung charakterisiert. Ausgewählte Proben wurden außerdem mittels Röntgendiffraktometrie (XRD), Transmissionselektronenmikroskopie (TEM) und Neutronenreflektometrie untersucht.

Die Messungen zeigen, dass die Beimischung von $^{11}B_4C$ die Güte der Proben drastisch verbessert. Außerdem haben sich modulierte Ionenunterstützung und Ionenunterstützung mit hohem Fluss als wichtige Methoden erwiesen, um polarisierende Vielschicht-Neutronenspigel von hoher Qualität herzustellen.

Abstract

This master thesis describes the principle, design, growth and characterization of polarizing multilayer neutron mirrors. Focus was put on optimizing growth parameters to minimize interface imperfections i.e. roughness and intermixing between the layers and to obtain high-quality neutron mirrors.

To create polarizing multilayer neutron mirrors one of the chosen materials has to be ferromagnetic. Furthermore, it is important that the nuclear Fermi-pseudopontential for the lower spin-state of the ferromagnetic partner has a similar value as the one of the non-magnetic material. Cobalt (Co) and Titanium (Ti) fulfill these requirements and were therefore chosen as the materials. The impact of adding isotope enriched low neutron-absorbing boron carbide ($^{11}B_4C$) during the growth of the multilayer on the obtained quality of the interfaces was thoroughly tested.

The multilayers were grown by ion-assisted direct current magnetron sputter deposition using two different deposition systems. The difference between continuous and modulated ion-assistance was examined. In the latter case the first part of each layer is grown using low-energy ion-assistance while the second part uses ions with a higher energy.

One of the deposition systems offered the possibility to grow multilayers with high-flux ion-assistance. This was used to examine the impact of different ion-fluxes on the quality of the multilayers.

The multilayers were primarily characterized using x-ray reflectivity (XRR) and x-ray diffuse scattering measurements. Selected samples were also characterized by x-ray diffraction (XRD), transmission electron microscopy (TEM), and neutron reflectivity.

It is shown that co-sputtering $^{11}B_4C$ during multilayer growth drastically improves the quality of the multilayers. Furthermore, ion-assistance modulation and the possibility to create high-flux ion-assistance have proven to be vital tools for the deposition of high-quality polarizing multilayer neutron mirrors.

Acknowledgements

Hereby I want to thank everybody who accompanied me for longer or shorter time periods during my whole studies and especially during the creation of this master thesis. I want to express my special gratidue to,

Fredrik Eriksson, my supervisor in Linköping for giving me the opportunity to perform such an interesting and cutting-edge research. Also thanks for his patience in guiding me, explaining every little detail, sharing his professional expertise and for all the time we spent together fixing Adam or staring full of hope at pressure displays and reflectivity curves.

Naureen Ghafoor for all her help, suggestions, inspiration and great knowledge. Also thanks for her willingness to explain how to solve Adam's pecularities even in her free-time at home and making sure that my pitiful attempts at TEM sample preparation, against all odds, did deliver useful results.

Gerald Badurek and Erwin Jericha who took on the challenge of supervising me while being more than 1 000 km away, without them this thesis would not have been possible.

My parents Maria and Wolfgang for offering support in all situations and making my studies and my stay in Sweden financially possible.

My brothers Mischa, Ma and Matti who were very helpful with all kinds of mathematical or administrational problems the university offered, especially in the first months of my studies.

Jakob, Luki, Alex, Berni and Hacki in place of all the fellow students in Vienna for making "Kreuzerlübungen" and studying for exams way easier.

Lukas, Robin, Maxime and Fan representing all the awesome people I got to know during my time in Linköping for constantly making sure that I did not spend too much time in the labs working on my thesis.

Anna for always being there for me, her endless patience, providing me a home and her ability to see a positive aspect in everything.

Contents

1 Introduction

Neutron physics is an ever-growing field since the discovery of the neutron in 1932 by James Chadwick. Because of its charge neutrality, the resulting deep penetration into matter, and the high mass, neutrons are popular in scientific applications, especially for the study of condensed matter, see e.g. [1–3].

For most purposes an exact knowledge and/or control of the characteristics of a neutron beam, like intensity, collimation, polarization and wavelength, is necessary. This is where multilayers come into play: they find usage as all kinds of neutron optical elements - monochromators, collimators, benders, filters, analyzers, polarizers and also as waveguides.

For this wide range of applications of multilayers in neutron optics they are required to be as ideal as possible, i.e. the interfaces between the two materials of which they consist should be smooth and flat with no intermixing or roughness even in very thin layers. Furthermore, it must be possible to have exact control over the parameters of the multilayers, like multilayer period and layer thickness ratio. To achieve that the way of creating the multilayers has to be perfected.

The most common method to grow multilayers is by sputter deposition which allows many parameters to be fine-tuned. To obtain the ideal conditions for the growth of multilayers several sets of samples were deposited to examine the effect of the different parameters.

Based on the neutron optical properties as materials cobalt and titanium were chosen to create the samples. The materials offer important features: A low neutron absorption when deposited as thin films, one of the materials has to be ferromagnetic (Co) to realize polarizing neutron mirrors and the Fermi-pseudopotential of Co for the lower spin-state is similar to the one of Ti.

A positive effect on the quality of the multilayers is observed when low neutron-absorbing isotope enriched $^{11}B_4C$ is co-sputtered during the deposition. Ion-assisted sputter deposition was tested using different values for the ion-energy and apart from that the difference between modulated ion-assistance and continuous ion-assistance was examined. Additionally, the impact of high-flux ion-assistance compared to ordinary, low-flux ion-assistance on the multilayer quality was analyzed.

The thesis at hand is the result of a five-month stay at Linköping University in Sweden and it is outlined as followed: the next chapter describes multilayer neutron mirrors in general and two special types, namely depth-graded supermirrors and periodic polarizing multilayer mirrors. The effect of roughness and intermixing in real multilayers and the reasons why cobalt and titanium were chosen are also part of this chapter.

The third chapter is devoted to the growth of multilayers by sputter deposition

and several techniques to improve the quality of the multilayers are explained. A detailed description of the two used deposition systems is given as well and in chapter four some of the challenges that one of the two systems brought up are described.

In chapter five an overview of the multilayers that were characterized using the techniques described in chapter six is found. The results of the characterization methods are summarized in chapter seven while the last chapter concludes the thesis and gives suggestions to subsequent analysis in this research field.

2 Neutron Mirrors

Neutron mirrors are most commonly used as waveguides to direct neutrons from a source to a distant place. Often several experiment setups are located around the same neutron source and the neutron beam has to be guided to the different experimental stations. Neutron mirrors with high reflectivity are required to ensure a sufficiently high amount of the generated neutrons can be used for the experiments.

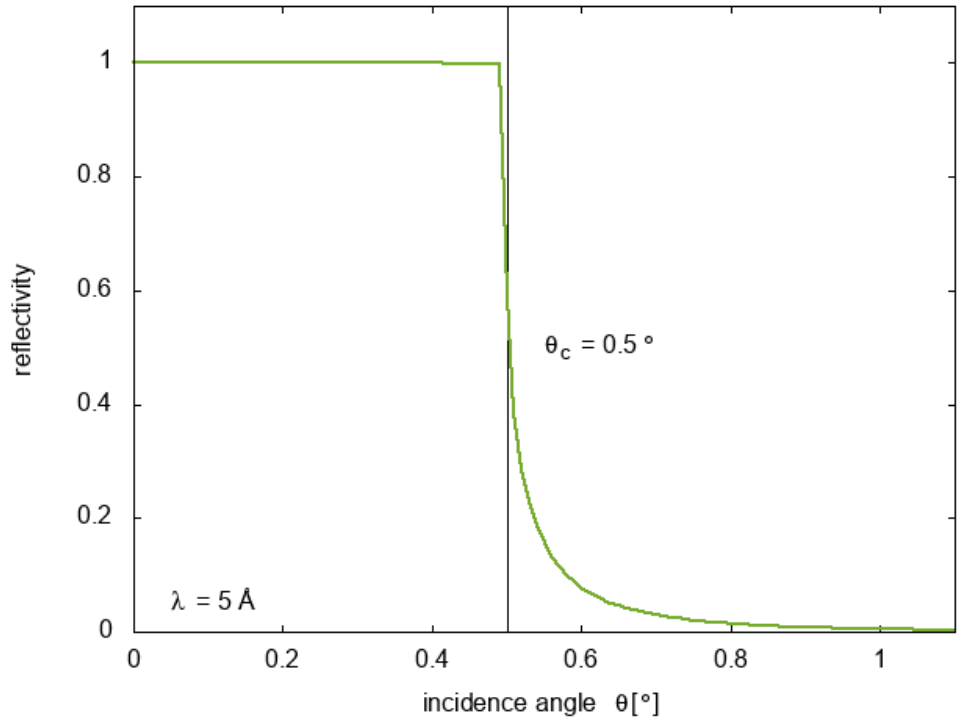

Figure 1: Simulation of the reflectivity R of a single nickel layer for a neutron wavelength of $\lambda = 5$ Å as a function of incidence angle θ. The simulation was carried out with the IMD software package developed by Windt [4]. For small incidence angles θ $R = 1$ is achieved, at $\theta = \theta_c = 0.5°$ the reflectivity drops to zero almost instantaneously.

Since neutrons can be described as particle waves they follow the same laws for reflection, including total reflection, as ordinary light waves. With a material that is optically thinner than vacuum total reflection of neutrons can be realized [5]. However, since the grazing incidence angle θ has to be smaller than a certain critical angle θ_c with respect to the surface to ensure total reflection for most applications neutron mirrors that rely only on total reflection are not good enough. The critical angle θ_c is wavelength dependent and generally has a low value, e.g. for a single Ni layer, which is the best natural neutron reflector, $\theta_c = \lambda[\text{Å}] \cdot 0.1° \text{Å}^{-1}$, see Fig. 1.

Since θ_c is very small it is desirable to manufacture optical elements that have

a good reflection also for $\theta > \theta_c$. By constructing a mirror consisting not only of one layer but of a series of parallel layers of different materials (usually two) with properly chosen layer thicknesses it is possible to realize mirrors with a high reflectivity above the critical angle.

These multilayer neutron mirrors have been used as monochromators or polarizers and, furthermore, so-called supermirrors have been created that reflect neutrons over a wide range of incidence angles. An introduction to the physics of the different kinds of multilayer neutron mirrors is given in the following sections.

2.1 Multilayer Neutron Mirrors

When treated as a particle wave a neutron can be ascribed an energy of

$$E = \frac{\hbar^2 k^2}{2m} + V \tag{1}$$

where $\hbar$ is Planck's constant divided by 2π, V is the potential in which the neutron is moving, k is the wave vector, and m is the neutron mass. The effective nuclear scattering potential of a medium can written as [6]

$$V_{nuc} = \frac{2\pi\hbar^2}{m} N_b = \frac{2\pi\hbar^2}{m} b_N \rho \tag{2}$$

with N_b being the scattering length density, ρ the number of nuclei per unit volume, and b_N the nuclear coherent scattering length. The latter is an empirical material-specific quantity which varies across the periodic table and for different isotopes of the same element and is positive for most materials [7] which also leads to N_b being positive for a wide range of materials.

When neutrons move from one medium to another some of the neutrons are reflected at the interface while others transmit into the new medium after being refracted. A neutron beam that is incident onto a multilayer consisting of N bilayers leads to the neutrons being effectively exposed to periodic square-well potentials. At each interface the beam is partly reflected and partly transmitted, see Fig 2. In order to have a high reflectance from the multilayer the reflected neutrons must interfere constructively.

The main geometric parameters of such a multilayer are the amount of bilayers N, the multilayer period Λ, and the layer thickness ratio $\Gamma = \frac{d_B}{\Lambda}$, which determines the thicknesses of the individual layers d_A and d_B with $d_A + d_B = \Lambda$. The shape of the created square-well potentials is determined by the geometry of the multilayer, see Fig. 2.

The reflection of a neutron beam from a multilayer mirror has similarities to the diffraction of x-rays, neutrons or electrons from a crystal lattice described by the well-known Bragg's law

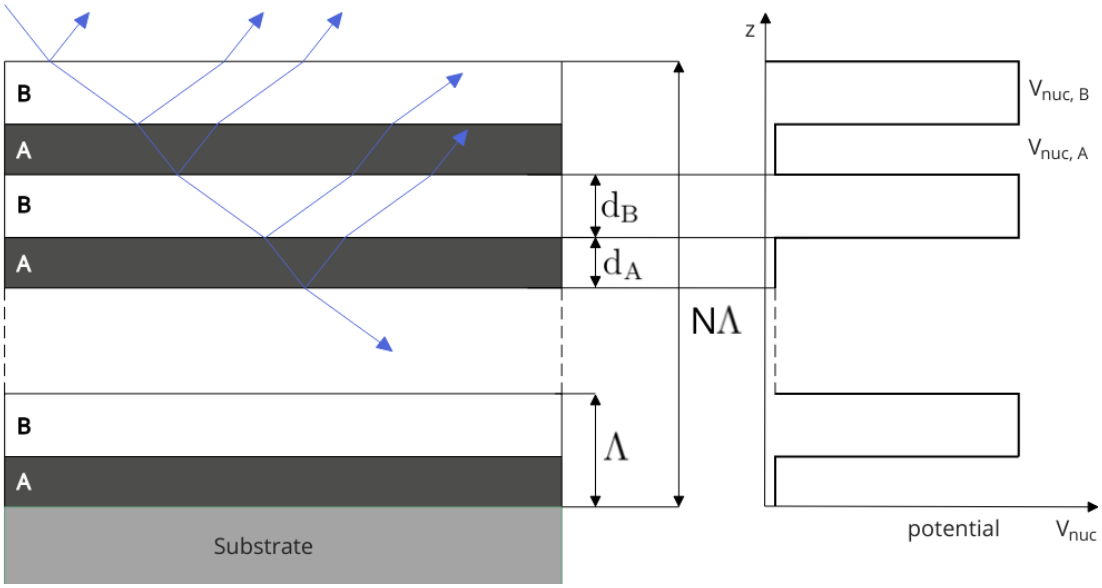

Figure 2: left: Illustration of the behaviour of a neutron beam that is incident onto a multilayer neutron mirror, at each interface the neutrons are either reflected or transmitted. right: the potential that is generated by an ideal multilayer neutron mirror. The height of the potential square-wells is determined by the chosen materials.

$$m\lambda = 2dsin\theta \tag{3}$$

where m is the order of reflection, d is the lattice spacing, λ the wavelength of the radiation, and θ the grazing incidence angle.

However, in the case of neutrons being *reflected* from a multilayer refraction has to be taken into account. This leads to a modification in Bragg's law

$$m\lambda = 2\Lambda \sin\theta \sqrt{1 + \frac{\bar{n}^2 - 1}{\sin^2\theta}} \tag{4}$$

where the multilayer period Λ takes the place of the lattice spacing d, and $\bar{n} = 1 - \bar{\delta}$ is the mean real part of the refractive index n

$$n = n(\lambda) = 1 - \delta + i\beta \tag{5}$$

of the multilayer. δ is called the dispersion and β the extinction coefficient and the mean real part of a multilayer consisting of material A and B is given by:

$$\bar{\delta} = \frac{d_A\delta_A + d_B\delta_B}{d_A + d_B} \tag{6}$$

In the same way as for x-rays neutron mirrors give rise to Bragg peaks in the reflectivity pattern when the reflected particle waves interfere constructively, see Fig. 3.

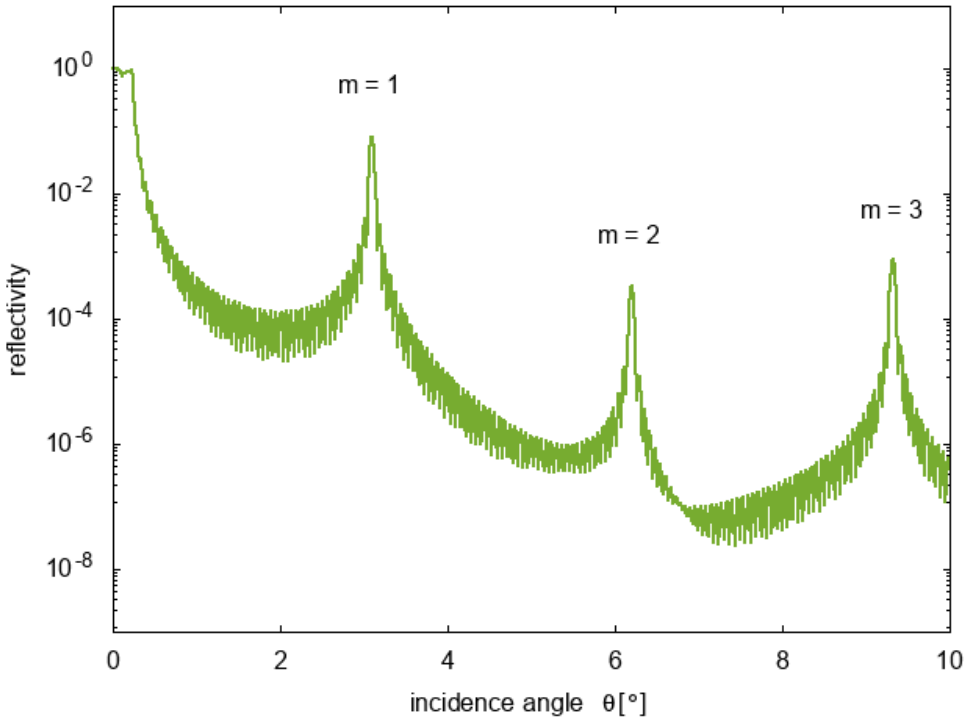

Figure 3: Neutron reflectivity simulation of a Co/Ti multilayer with the parameters $N = 50$, $\Lambda = 48$ Å *and* $\Gamma = \frac{d_{Ti}}{\Lambda} = 0.46$. *The first three Bragg peaks at* $\theta = 2.98°$, $5.98°$ *and* $8.99°$ *for* $m = 1, 2, 3$, *respectively, are clearly visible.*

As was shown by Saxena and Schoenborn in 1977, the reflectivity is directly proportional to N^2 and increases with increasing difference in the potentials of the two materials [8]. Since the potential of a medium is directly proportional to the scattering length density, see Eq. (2), the materials are chosen to have a large difference in their respective values for N_b to ensure a high reflectivity of the neutron mirror.

2.2 Neutron Supermirrors

Neutron mirrors consisting of bilayers with constant thicknesses throughout the multilayer are suitable as monochromators if the multilayer parameters are carefully selected. To reflect neutrons over a range of incidence angles so-called supermirrors were developed, where the layer thicknesses vary throughout the multilayer stack.

The difference of neutron supermirrors to ordinary multilayer neutron mirrors is that for supermirrors the period is varied giving the multilayer an aperiodic geometry, as was first suggested by Mezei [9]. Fig. 4 gives an illustration of a neutron supermirror.

Regular multilayer neutron mirrors reflect only neutrons when their respective

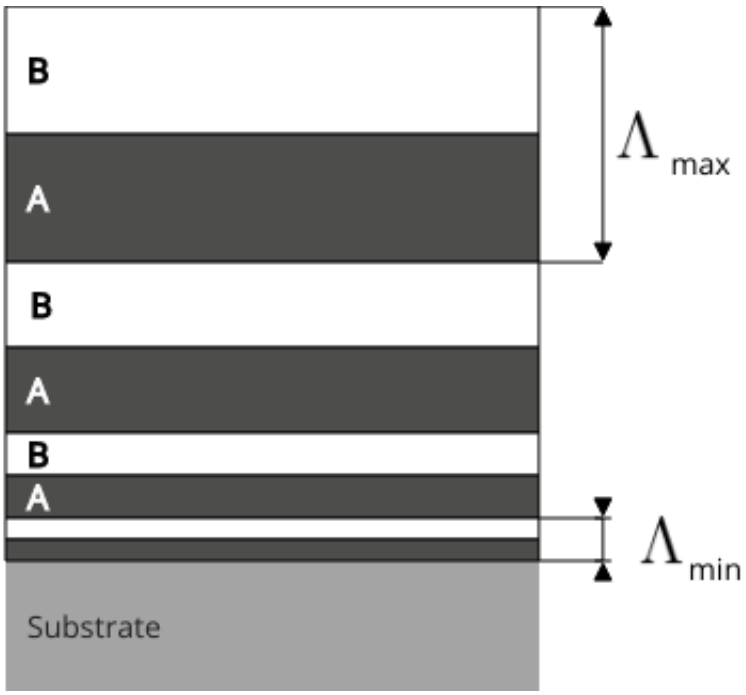

Figure 4: Illustration of a neutron supermirror with varying Λ leading to an aperiodic geometry.

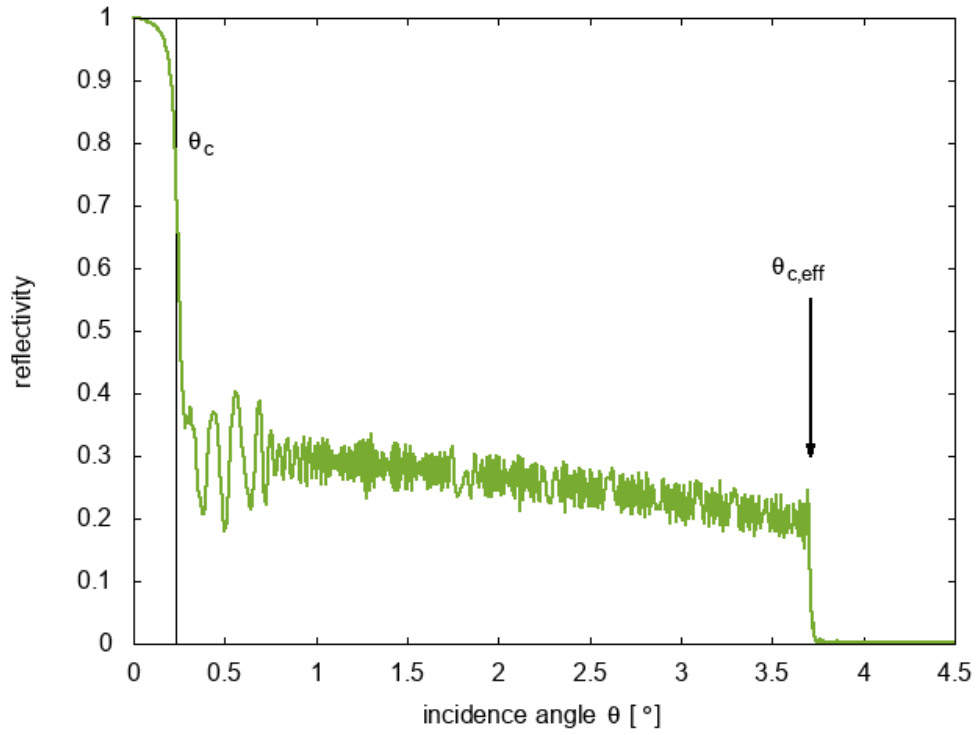

Figure 5: Simulation of the neutron reflectivity of a Co/Ti supermirror with $N = 5000$ and $\lambda = 5.183$ Å. It has to be noted that the depth-grading was not opimized which is why there is a drop in reflectivity at the critical angle for total reflection.

incident angle fullfills the Bragg condition. Since in neutron supermirrors the period is gradually varied throughout the multilayer the individual Bragg peaks of the different bilayers overlap, creating a neutron mirror that reflects either neutrons with the same wavelength over a whole range of incident angles, see Fig. 5, or neutrons with the same incidence angles over a range of wavelengths.

The thickness of the thinnest layer in the supermirror determines the highest possible value for the effective critical incident angle $\theta_{c,eff}$ at which the neutrons are still reflected for a fixed wavelength. To characterize a multilayer neutron supermirror the so-called m-value is introduced which is the ratio of its effective critical angle to that of natural nickel

$$\theta_{c,eff} = m\theta_{c,Ni} \tag{7}$$

For most applications a high value for $\theta_{c,eff}$, i.e. a supermirror with a high m-value, is desired. This means a lot of effort is put into the research to create multilayers with as small multilayer periods as possible.

2.3 Polarizing Multilayer Neutron Mirrors

Polarizing multilayer neutron mirrors were first reported by Lynn et al. in 1976 [10]. The basic idea is to create different potential landscapes for spin-up and spin-down neutrons to reflect one and transmit the other.

To create different potential shapes for the two different spin-states a magnetized ferromagnetic material for one of the two materials that make up the multilayer is used. The spin of a neutron will lead to magnetic scattering between the magnetic moment of the neutron and that of the atoms in the ferromagnetic material, therefore, the potential in Eq. (2) has to be modified. For this reason the magnetic optical potential, V_m, is introduced

$$V = V_{nuc} + V_m = \frac{2\pi\hbar^2}{m} b_N \rho - \mu B = \frac{2\pi\hbar^2}{m} \left(b_{nuc} \pm b_m\right), \tag{8}$$

where μ is the neutron's magnetic moment, B is the saturated magnetic induction, and $b = b_{nuc} \pm b_m$ is the total scattering length consisting of a nuclear b_{nuc} and a magnetic part b_m. The plus and minus sign in Eq. (8) differentiate between the cases of the neutron spin being parallel and antiparallel to the direction of magnetization of the magnetic mirror. A potential created by a neutron polarizing multilayer mirror is shown in Fig. 6.

Since the reflection of a neutron that hits a multilayer is dependent on the contrast of the potential spin-up and spin-down neutrons will be affected in different ways. Neutrons with their spin parallel to the magnetic field are exposed to a high contrast in the square-well potentials and will be reflected with a high probability.

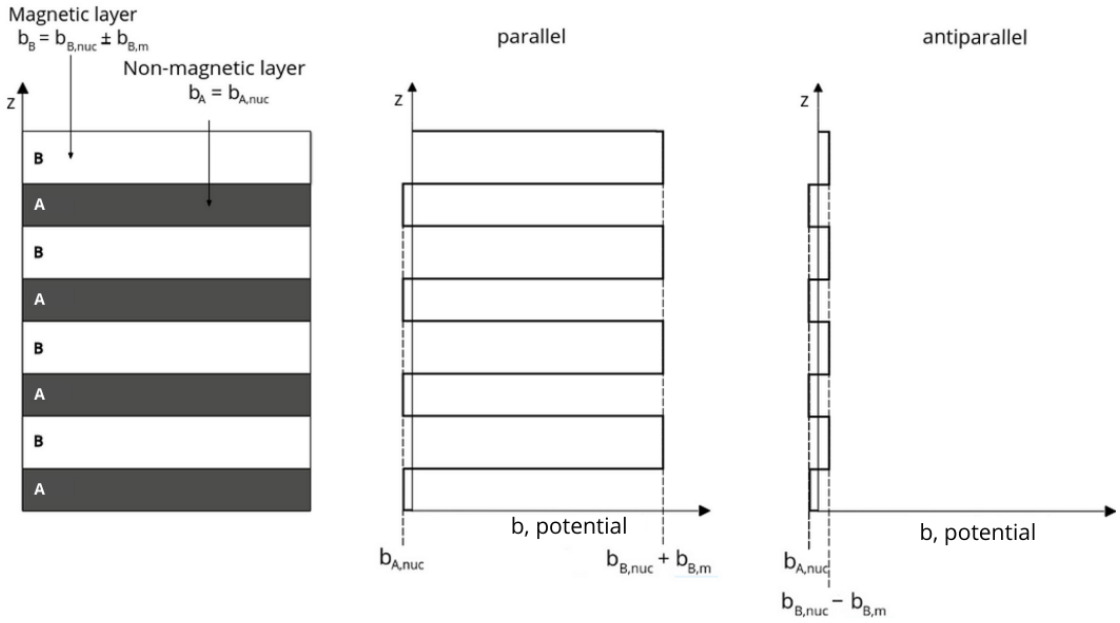

Figure 6: A polarizing multilayer neutron mirror (left) and its total scattering length for neutrons where the spin is parallel (center) or antiparallel (right) to the magnetic field of the ferromagnetic layer. In the first case the high contrast in the potential will lead to reflection while in the second case the neutrons will be transmitted.

Neutrons with an antiparallel spin on the other hand experience almost no contrast and will therefore most probably be transmitted.

With the correct materials and a suitable magnetization a polarizing multilayer neutron mirror only reflects neutrons with one spin-state while transmitting the others which leads to a high polarization in the reflected neutron beam.

2.4 The Role of Imperfections

A real multilayer differs from an ideal one in some aspects; for example the interfaces between the two materials are never ideally flat or perfectly parallel on an atomic level.

Roughness and interdiffusion at an interface lead to a deviation of the generated potential from the ideal square-well shape [11] and therefore decrease the overall performance of the neutron mirror. The interface width is a limiting factor when trying to generate better neutron mirrors or supermirrors with high m-values.

A common way to define the interface width is to describe the refractive index at the boundary of the two materials i.e. if it is abrupt, continuous, steplike or a combination of these. The normalized average of the refractive index along the growth direction z is the so-called interface profile function $g(z)$. Its spatial

derivative

$$f(z) = \frac{g(z)}{dz}, \tag{9}$$

is then used to define the interface width 2σ, an average amplitude of surface height fluctuations, see Fig. 7

$$\sigma = \int z^2 f(z) dz. \tag{10}$$

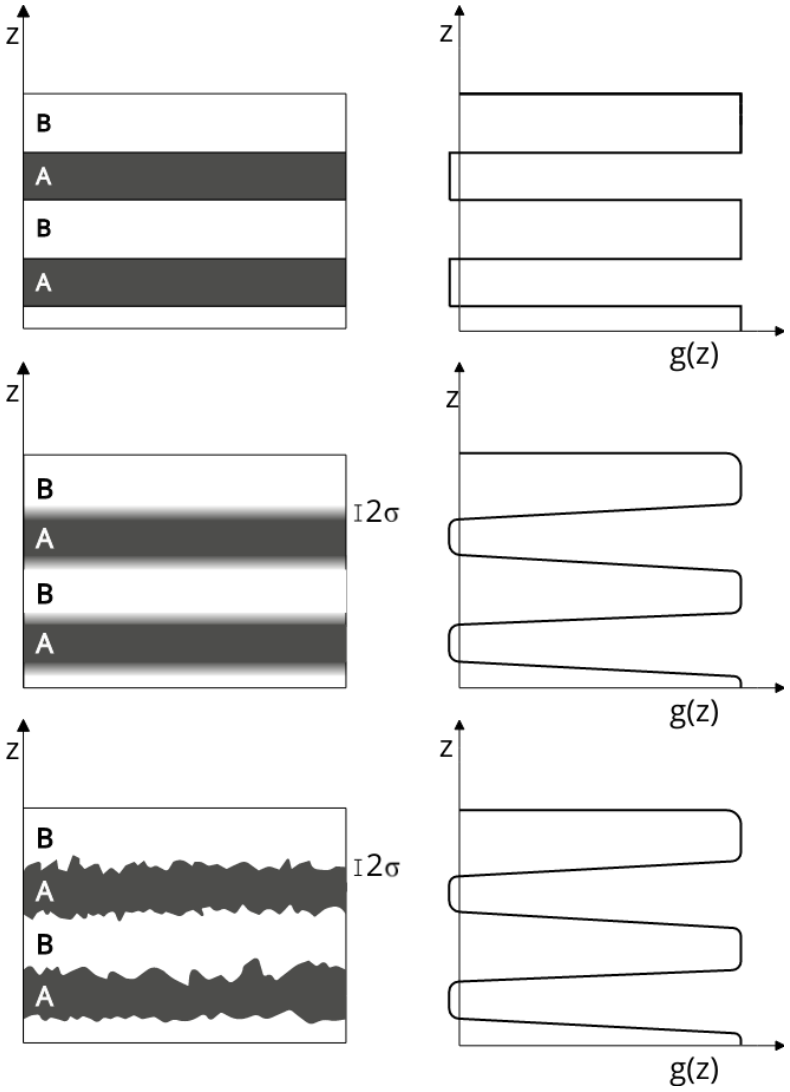

Figure 7: Multilayer neutron mirrors and their respective interface profile function; for an ideal multilayer (top), intermixed interfaces (center) and rough interfaces (bottom).

The effect of roughness and intermixing is often taken into account using the root mean square roughness, σ in a Debye-Waller model [12]. In this model the reflectivity R amounts to

$$R = R_0 \exp\left(-\left(\frac{4\pi\sigma \sin\theta}{\lambda}\right)^2\right) \tag{11}$$

where R_0 is the theoretical reflectivity for ideal interfaces and θ and λ are the glancing angle and the wavelength of the incident neutron beam, respectively.

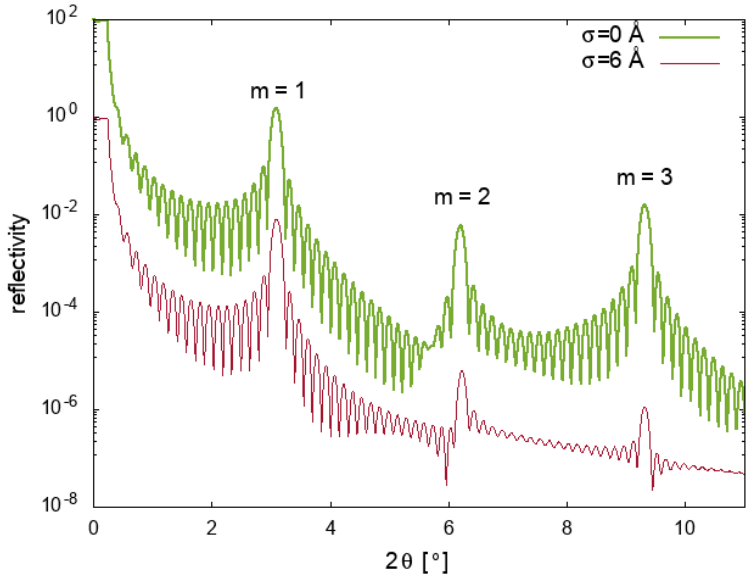

(a) neutron reflectivity vs. angle of incidence for two different values of σ

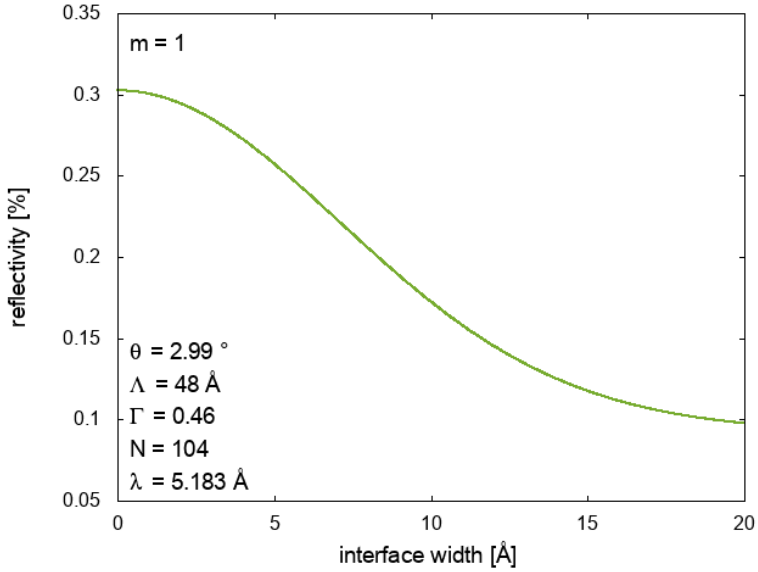

(b) neutron reflectivity vs. σ

Figure 8: IMD-simulation of the neutron reflectivity of Co/Ti mirrors. The simulated multilayers consisted of $N = 104$ layers with $\Lambda = 48$ Å and $\Gamma = 0.46$, the neutron beam had a wavelength of $\lambda = 5.183$ Å. (a) Reflectivity as a function of the incidence angle for $\sigma = 0$ Å (shifted vertically 100 times) and $\sigma = 6$ Å. The Bragg peaks are significantly weaker pronounced with increasing values for σ. (b) Reflectivity as a function of the average interface width σ with an incidence angle $\theta = 2.99°$ which is the position of the first Bragg peak. As expected, the reflectivity decreases with increasing values for the interface roughness σ.

An obvious disadvantage of this model is that it does not offer any possibility of discriminating between intermixing and roughness for multilayer structures. In a real multilayer the roughness scatters neutrons away from the specular direction while intermixing attenuates the reflectance.

Fig. 8 shows the effect of imperfect interfaces on the reflectivity of a Co-Ti neutron mirror. It can be clearly seen that σ has a strong negative influence on the reflectivity. This impact is even more prominent for multilayers with low values of Λ which are needed for the creation of neutron supermirrors with a high m-value.

Since a high σ reduces the reflectivity drastically, see Eq. (11), the multilayers are required to have sharp and smooth interfaces and σ should be completely eliminated or at least as small as possible.

To reduce the troublesome effect of deviations from ideal interfaces between the two materials the method of fabricating the multilayer has to be chosen carefully and possible problem-causing effects have to be eliminated thoroughly. For more details regarding the fabrication of the multilayers and improvements to the ordinary method see section 3.

2.5 Material Selection for Polarizing Multilayer Neutron Mirrors

Non-polarizing multilayer neutron mirrors and supermirrors have been realized using several different material combinations such as Ni/Ti [13–18], NiC/Ti [12, 16, 19, 20] or Mn/Ge [8, 21]. Since the aim of this work is to investigate polarizing multilayer neutron mirrors, one of the materials has to be ferromagnetic to create a potential that is different for the two spin-states of a neutron.

Another aspect that has to be kept in mind when selecting the materials is that, as explained in previous sections, the reflectivity depends heavily on the contrast in the scattering lengths of the two materials. Therefore, the two materials should exhibit a large difference in their respective scattering length densities.

Furthermore it has to be considered that the imaginary part of the scattering length density of the chosen materials has to be small since that corresponds to neutron absorption which should be kept as low as possible.

The last two aspects can be examined by plotting the real versus the imaginary part of the scattering length density of the materials that are possible candidates, see Fig. 9.

Today, most neutron polarizing multilayer mirrors are manufactured using Co/Ti [22–25], Fe/Si [26, 27] or Fe/Ge [28, 29] multilayers. Due to time restrictions only one material combination could be examined for this work which was chosen to be Co/Ti.

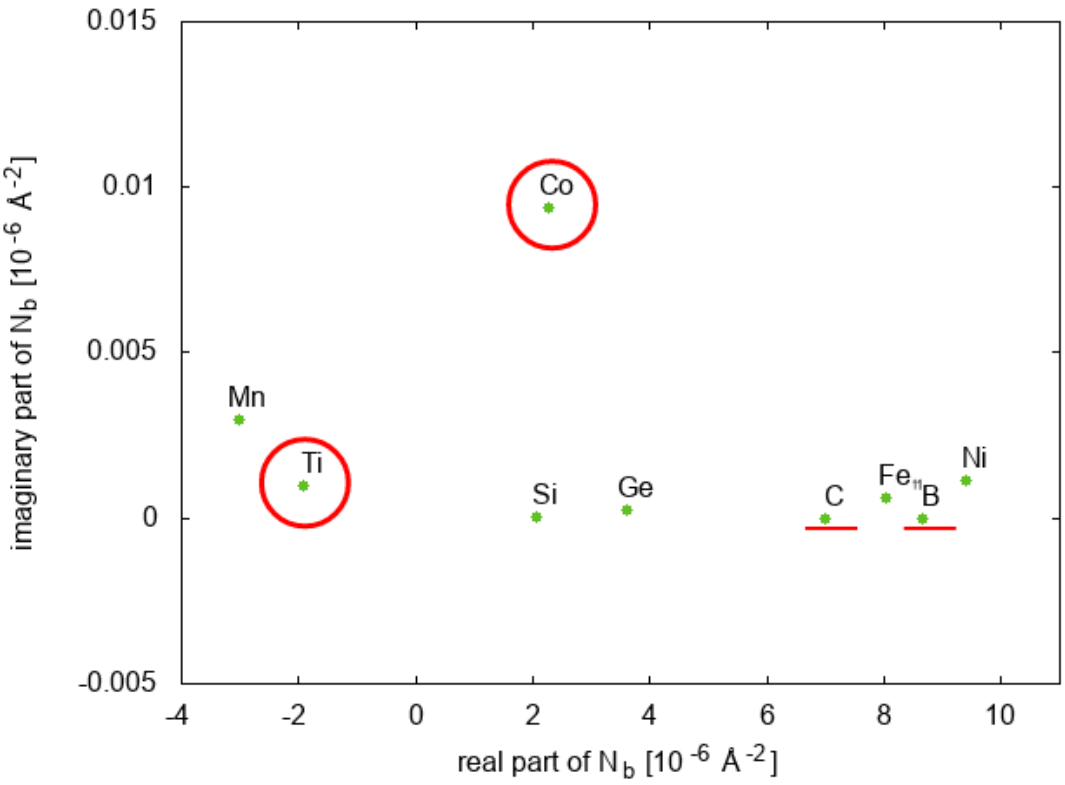

Figure 9: The imaginary versus the real part of the scattering length density for selected materials. For the fabrication of neutron polarizing multilayer mirrors one of the chosen elements has to be ferromagnetic. Both elements are required to have a low imaginary part of the scattering length density while the contrast in the real part should be as high as possible. In the graph it seems that Co has a high absorption which is due to the fact that only a small part of the whole graph is visible and the axes have different scales. All of the shown materials exhibit a very low value for the imaginary part of their respective scattering length density.

As was shown by Ghafoor et al. [30] co-sputtering, see Sec. 3.3, of B_4C during the growth of Cr Sc multilayers, which were intended as x-ray mirrors, prevents the formation of crystalline grains. The stabilization of an amorphous layer structure by using B_4C improved the performance of the mirror because the amorphous layers enabled lower interface roughness and smoother interfaces.

Since smoother interfaces are also desired in multilayers used as neutron mirrors, see Sec. 2.4, the effect of incorporation of isotope-enriched $^{11}B_4C$ into the Co and Ti layers on structure and performance of the neutron mirror was also investigated in this work. $^{11}B_4C$ was used since natural B contains $\sim 80\%$ of ^{10}B which is strong neutron-absorbing while ^{11}B is low neutron-absorbing.

2.6 State-of-the-Art and Current Limitations

Today the highest m-value reached for supermirrors is $m = 8$ with $R = 0.4$ for a Ni/Ti multilayer, as was published by Schanzer et al. in 2016 [31]. In the same work a polarizing Fe/Si supermirror with $R = 0.7$ at $m = 5.5$ and a polarization of $P \sim 1$ over the entire supermirror regime was presented, see Fig. 10.

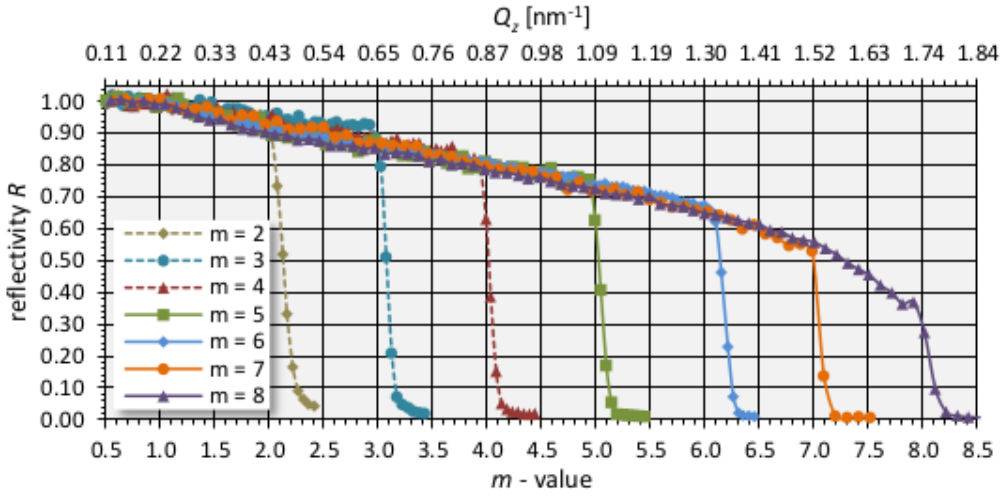

(a) Reflectivity of supermirrors with $2 \leq m \leq 8$

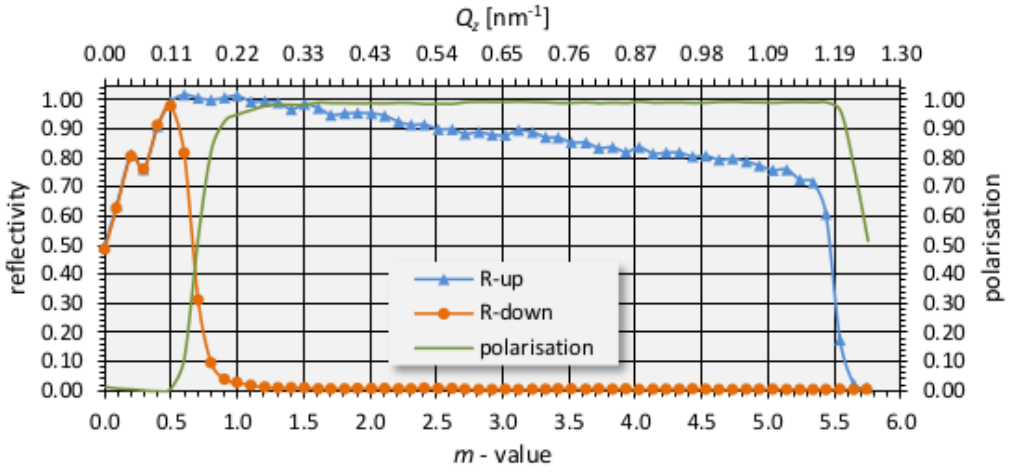

(b) Spin-dependent reflectivity and polarization

Figure 10: The reflectivity of (a) Ni/Ti supermirrors and (b) of a polarizing $m = 5.5$ Fe/Si supermirror as reported in [31].

To make supermirrors with $m = 8$ the thickness of the thinnest layer has to be $d \sim 18$ Å. When trying to reach even thinner layers the interface roughness becomes more and more prominent, limiting the performance of the neutron mirror.

Another limitation when trying to reach higher m-values is that the number of layers N that are needed increases drastically with higher m-values, approximately desribed by $N = 4m^4$ [31]. Thus, this requires the $m = 8$ supermirror to consist of more than 16 000 layers. This huge amount of layers gives rise to a whole range of

problems like accumulated roughness and induced stress leading to delamination.

Another problem that emerges from high values for N is reported to be absorption [31]. After a certain amount of layers all the neutrons are either reflected or absorbed and do not reach the bottommost layers which makes them useless. Although the materials are chosen to exhibit only a small imaginary part of their respective scattering length density which corresponds to absorption a non-negligible amount of the neutrons are absorbed.

For Co/Ti multilayers it has been reported that the formation of crystalline grains which diffract the neutrons and, therefore, limit the performance of neutron mirrors [25] is another problem. There have been attempts to limit crystalline formation by depositing the multilayers using reactive sputtering but no method has been found to ensure an amorphous layer structure throughout the whole multilayer.

3 Sputter Deposition

Sputter deposition is a technique that is widely used for the fabrication of multilayers, see e.g. [23–25, 30, 32]. With some additions to the basic idea it is possible to create multilayers with flat and sharp interfaces with good control of the thicknesses of the individual layers.

For sputter deposition the material that is to be deposited, usually called target, is placed in a vacuum chamber together with the substrate. A so-called working gas, e.g. argon, is admitted into the chamber and a highly negative charge is applied to the target. This affects the few electrons and ions that are present in the gas because of cosmic radiation and electrons being emitted from the negatively charged target. The electrons are repelled from the target, collide with the gas atoms and ionize them with a certain probability due to electron impact ionization.

Subsequently, the positively charged ions are attracted towards the target at a very high velocity. Because of this bombardement a cascade of collisions takes place within the target and atomic particles of the target material are, among others, ejected i.e. "sputtered off" the target. These target atoms cross the vacuum chamber and are deposited on the substrate as a thin film. In most sputter deposition systems the substrate rotates to ensure a uniform thickness of the film.

When the ions hit the target so-called secondary electrons are also sputtered off besides the neutrally charged atoms. These electrons will lead to further gas ionization and increase the efficiency of the process. The energy with which the ions hit the target has to be chosen to fit the target material and can be controlled by varying the target's potential. Fig. 11 shows an illustation of the sputter deposition process.

Since the electrons are mostly generated by the ions hitting the target and the ions are generated by gas atoms colliding with electrons there will be a certain amount of both kinds of particles where equilibrium is reached. In that case a plasma, i.e. a quasi-neutral gas of charged and neutral particles, is sustained. Because of electron excitation of the gas atoms, photons will be emitted in the relaxation process leading to a visible glow of the plasma, see Fig. 12a.

In order to deposit multilayers using this technique two (or more) targets are placed in the chamber. By shutters that conceal the targets when closed, the material and deposition time during sputtering can be controlled. By timing the shutters it is possible to grow a multilayer with the desired layer thicknesses.

Before the working gas is admitted into the chamber the pressure, i.e. the background pressure, should be low to avoid contamination. Furthermore, the sputtering gas pressure has to be low to ensure that the sputtered atoms have a high enough mean free path to reach the substrate.

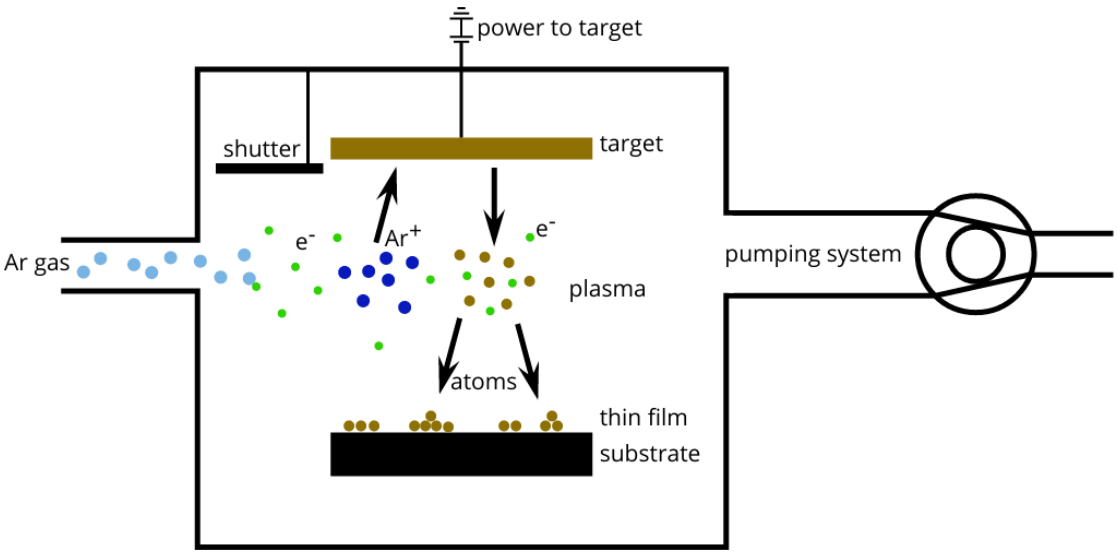

Figure 11: Illustration of a sputtering system. The working gas (light blue dots) is admitted into the evacuated chamber and with some probability ionized (dark blue) by collisions with electrons (green). Because of the target's negative potential the ions are accelerated towards it and sputter off more electrons and also atoms of the target material (brown) which then are deposited on the substrate (black).

3.1 Magnetron Sputter Deposition

In conventional sputter deposition the obtained growth rates are normally low and the growth of the film is slow. This can be compensated by placing magnets behind the target to generate a magnetic field that traps the electrons in circular paths close to the target because of the Lorentz force. This forces the electrons to cover a longer distance near the target which leads to a higher ionization rate of the working gas in that area. With this so-called magnetron sputtering the flux of ions which hits the target and hence the number of the sputtered atoms is increased which leads to higher sputtering rates.

3.2 Ion-assisted Sputter Deposition

The multilayers must have abrupt and flat interfaces for most applications. A rotating substrate improves the thickness uniformity but is not enough to ensure flat surfaces. On an atomic scale there will still be roughness because the energies of the atoms arriving at the substrate are normally not sufficient to provide enough surface mobility to grow smooth surfaces.

One possibility to improve the smoothness of the layers is to increase the surface mobility of the atoms in the growing film. This can be achieved by not only bombarding the target but also the growing film with ions from the plasma by

applying a negative bias to the substrate. During this "ion-assisted sputter deposition" the ion bombardement of the substrate has to happen at lower energies than the bombardement of the target to avoid re-sputtering and intermixing of the different layers. For a more detailed description of ion-assisted sputter deposition see e.g. [33].

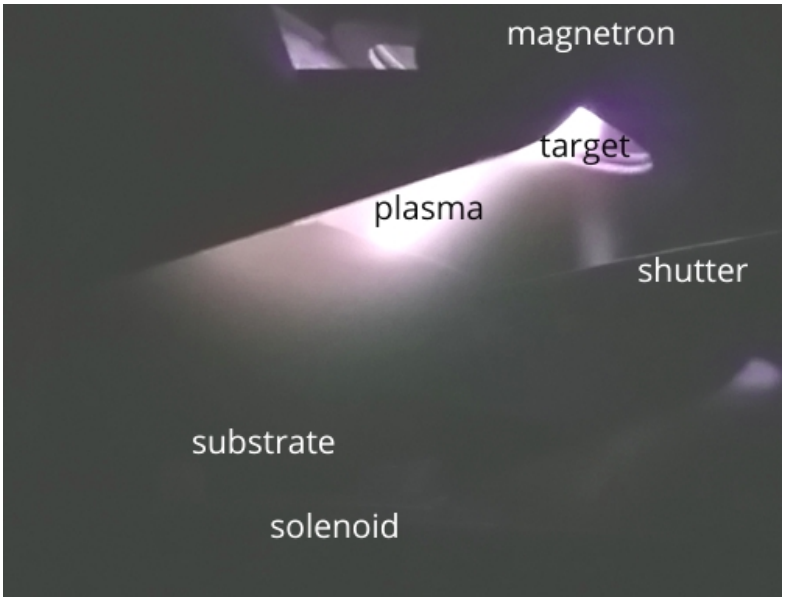

(a) low ion flux

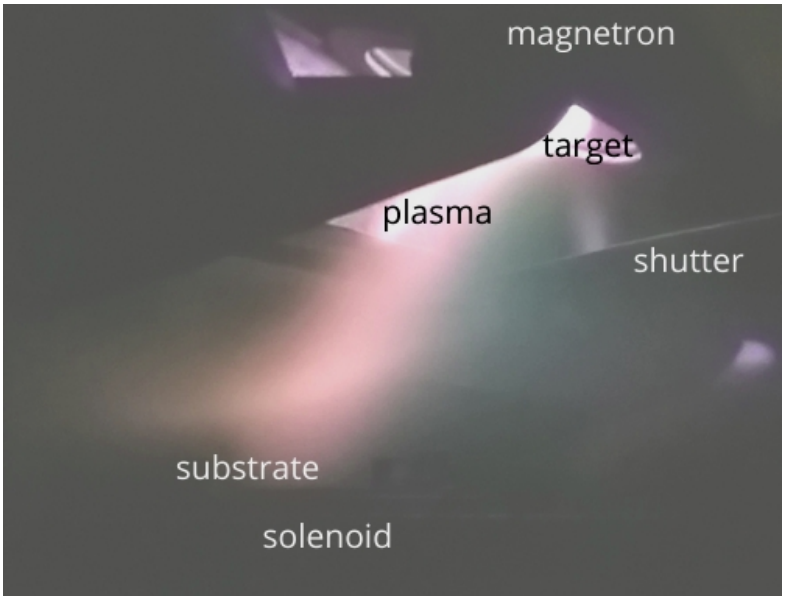

(b) high ion flux

Figure 12: Magnetic field configurations inside the deposition chamber. (a) Without solenoid coupling, (b) magnetron is coupled with the solenoid guiding more ions towards the substrate.

Since the bombardement of the growing film with ions has to happen at low energies, to improve the results of ion-assisted sputtering the flux of the ions hitting

the substrate has to be increased to ensure enough surface mobility of the atoms in the growing film. By placing a solenoid around the substrate which generates a magnetic field axially through the substrate position and selecting the correct direction of the solenoid current the secondary electrons of one of the targets can be guided towards the substrate. This ensures a high ionization rate in this region and therefore increases the ion flux that reaches the substrate and can be seen in the plasma glow close to the substrate, see Fig. 12b.

The ion-assistance can be improved even further by varying the energy of the ions that hit the film during the growth process. The first part of each layer should be grown with little or no ion-bombardement to avoid intermixing with the underlying layer. The second part of each layer should then be grown with a higher ion energy, densing the first part (ideally without intermixing), and smoothly terminating the surface before the next layer in the multilayer sequence is grown, see Fig. 13. More detailed information about this so-called "modulated ion-assisted sputter deposition" can be found in e.g. [34].

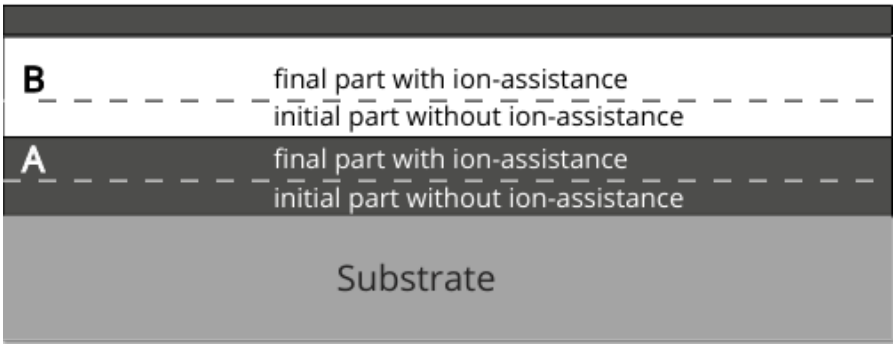

Figure 13: Schematic illustration of the principle of modulated ion-assistance.

3.3 Co-sputtering

In conventional sputtering all the targets are concealed by shutters except for one which corresponds to the target that is deposited at the moment. In some cases it might be desirable to create a compound of more than one material as the film. This is achieved by opening two or more shutters at the same time leading to multiple target materials being deposited simultaneously. During this so-called "co-sputtering" the stoichiometry is controlled by optimizing the magnetron power of each target seperately.

3.4 The Deposition Systems

The depositions were carried out using two different deposition systems: one located at the synchrotron source PETRA III at the Deutsches Elektronen-Synchrotron

(DESY) in Hamburg, Germany, and the second one at Linköping University (LiU), Sweden. In the following the main characteristics of both systems are outlined.

3.4.1 The Deposition System at DESY

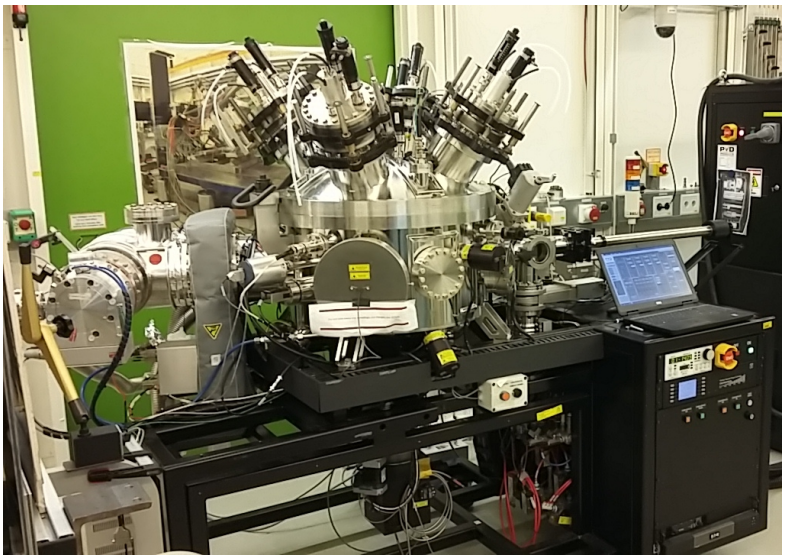

(a)

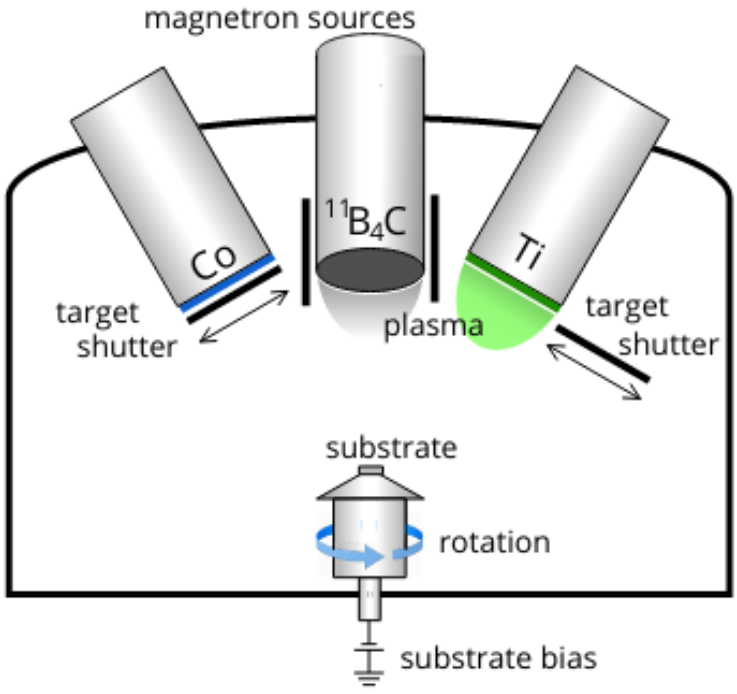

(b)

Figure 14: The deposition system at Petra III, Germany: (a) picture, (b) schematic illustration of the chamber, the unused fourth magnetron is not included for simplicity.

This deposition system offers the possibility to load four different 75 mm diameter targets tilted at an angle of 35° at the top of the chamber at the same time. Via

computer controlled shutters the currently deposited material is selected, however, for this work only three targets, namely Co, Ti and $^{11}B_4C$, were needed.

The distance between the target and the substrate can be varied manually between 130 and 230 mm. The chamber is cylindrical with a diameter of 600 mm to avoid interaction between sputtering sources and chamber walls. Two turbopumps and an integrated bake-out system offer the possibility to achieve a background pressure in the ultra-high vacuum (UHV) regime. However, since the chamber was left open for a long time before use and there was limited time for pumping the depositions were performed at a background pressure of $2 \cdot 10^{-8} - 8 \cdot 10^{-7}$ Torr ($2.6 \cdot 10^{-6} - 1 \cdot 10^{-4}$ Pa). Ar sputtering gas was introduced into the chamber to a working gas pressure of 3 mTorr (~ 0.4 Pa). During depositions the substrate was rotated at a constant speed of 10 rpm to ensure a good thickness uniformity.

This deposition system is also described in detail in [35]. For a picture and a schematic illustration of the deposition system see Fig. 14a and Fig. 14b, respectively.

3.4.2 The Deposition System at LiU - Adam

The second deposition system that was used during this thesis is a home-built system called "Adam" and offers a cylindrical chamber with a diameter of 500 mm and a height of 350 mm with a target-to-substrate distance of 120 mm. Two 75-mm-diameter magnetrons with a tilt angle of 25° against the substrate table normal are placed at the top of the chamber, see Fig. 15a for a picture of the deposition system.

Additionally, a third sputtering source with a diameter of 50 mm and the same angle is built in which was intended to be used to co-sputter $^{11}B_4C$. This third magnetron, however, gave rise to a lot of problems, see Sec. 4, and, therefore, co-sputtering of $^{11}B_4C$ was not possible with this system during this work.

Fast acting computer controlled shutters in front of the two bigger targets were used to sequentially deposit Co and Ti. These shutters allow for very accurate control of deposition times down to fractions of a second which is crucial to obtain the desired layer thicknesses. The 50 mm target has a manually controlled shutter which is the reason why it was intended to be used to co-sputter $^{11}B_4C$ so that the shutter can remain open during the whole time of the multilayer growth.

A major advantage of this system is a solenoid that surrounds the substrate table. Via magnetic coupling to the outer poles of the magnetrons, secondary electrons can be guided to the substrate vicinity where they ionize atoms of the working gas and, therefore, high-flux ion-assisted growth, as described in Sec. 3.2, can be realized, see Fig. 15b.

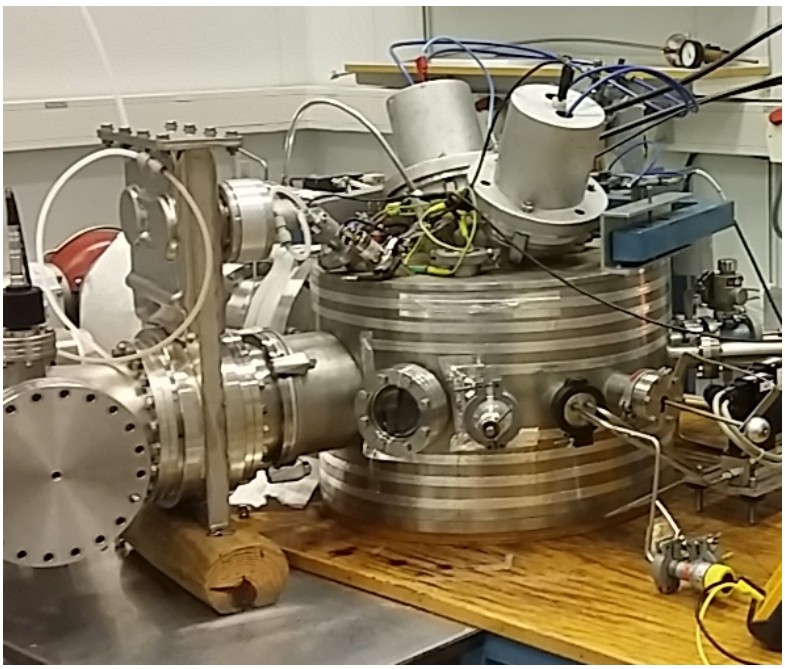

(a)

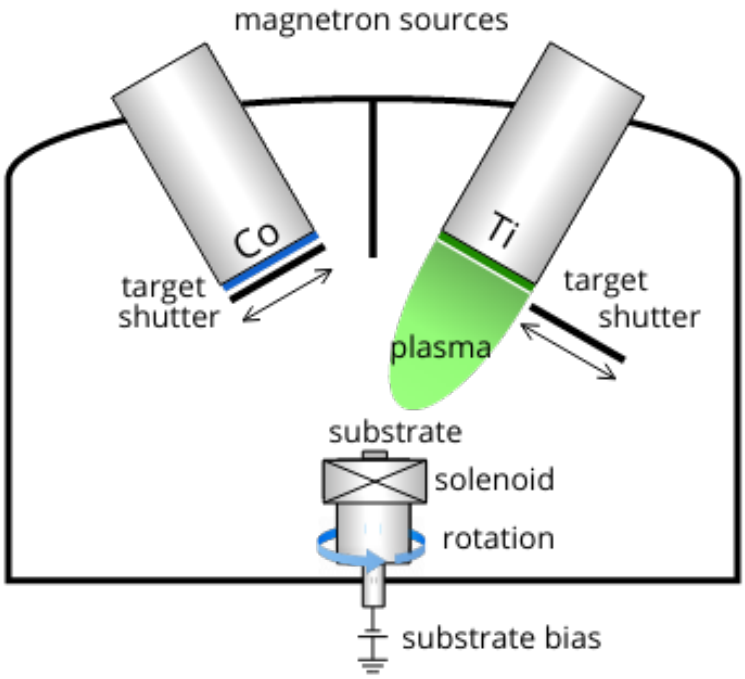

(b)

Figure 15: The deposition system at Linköping University, Adam: (a) picture, (b) schematic illustration of the chamber. For simplicity the unused third magnetron is not included.

The sputtering gas was again Ar with a pressure of 3 mTorr ($\sim 0.4\ Pa$). In contrast to the other system used, Adam can reach high vacuum only and not UHV and the depositions were performed at a background pressure of $\sim 2 \cdot 10^{-6}$

Torr ($2.7 \cdot 10^{-4}$ Pa). Again the substrate table rotated constantly during deposition with a speed of ~ 30 *rpm*. For more details regarding this deposition system see e.g. [30, 34, 36, 37].

4 Technical Issues

During the work for this thesis a large portion of the time was spent solving a wide range of problems with the deposition system in Linköping. In the following the main challenges and, if existing, their solutions are listed.

- The feedthrough for the substrate rotation was not tight and air leaked into the chamber. A new rotary feedthrough was ordered.
- Since the new rotary feedthrough did not have the same dimensions as the previous one an adapter was specifically designed and built to solve the problem.
- The substrate table did not rotate at constant speed but tended to get stuck. De- and remounting it fixed the failure.
- The shutter of one of the 75 mm magnetrons covered a part of the other target. This was solved by disassembling and readjusting the moving parts of the shutter system.
- The substrate bias did not behave as expected and, therefore, the ion-assistance could not be controlled adequately. A redesign of the electrical control system solved the problem.
- The 50 mm $^{11}B_4C$ target broke and the only replacement that was available was too thick. Gluing the pieces onto the backplate did not work but carefully fixing the broken parts in the magnetron proved to be a solution.
- The Co target ran out of material and the Cu plate that connects the target to the power supply was already being sputtered. The target had to be replaced with a new one.
- The original 50-mm-magnetron intended for $^{11}B_4C$ was leaking and did not allow the pressure in the chamber to reach a satisfying value. A replacement magnetron was installed.
- With the new 50-mm-magnetron no plasma could be ignited. The original magnetron was dismantled and redesigned several times using parts of a third magnetron to make sure that it was not leaking anymore.
- The cooling system of the 50-mm-magnetron was leaking and water escaped the magnetron outside the vacuum system. The magnetron was dismantled again and new connections for the cooling system were welded.

- With the new design for the cooling system of the 50-mm-magnetron the pressure in the chamber did not reach satisfying values when the cooling water was turned on. Due to time constraints this was the ultimate reason to omit co-sputtering $^{11}B_4C$ in the samples deposited with Adam.

These and a lot of other smaller problems made it necessary to vent and pump the system countless times, already created samples had to be redone and ongoing depositions stopped.

In the end the repair took so much time that the amount of samples deposited in Linköping had to be drastically reduced and they could only be deposited without co-sputtering $^{11}B_4C$. It shall be noted that shortly after finishing this thesis it was decided to order a completely new 50 mm magnetron to make co-sputtering with this deposition system possible.

5 Deposited Samples

The samples were deposited during two different time periods. The first series of samples was deposited in Hamburg, Germany during the early times of this work. In a second deposition period the system at LiU was used. See Sec. 3.4.1 and Sec. 3.4.2 for details about the two deposition systems.

All of the multilayers were deposited on Si(100) substrates with a native oxide. The substrates were chemically cleaned in consecutive ultrasonic baths of trichlorethylene, acetone and ethanol for about ten minutes each.

Not included are the samples which were used for rate calibrations and fine-tuning of the calculated rates, see Sec. 6.1.1 and 6.1.2.

5.1 Samples Deposited in Hamburg

The main purpose of these samples was to test the deposition of Co/Ti multilayers with co-sputtered $^{11}B_4C$ and to create samples that could be measured during beamtime at the neutron beam at the Institut Laue-Langevin in Grenoble.

The target powers were 60, 30 and 35 W for Ti, Co and $^{11}B_4C$, respectively. All samples were grown using modulated ion-assistance with a 10 Å thick initial layer grown with -30 V bias and the final layer with -100 V substrate bias.

- Two Co/Ti multilayers were stacked on top of each other with different multilayer periods, $\Lambda_1 = 50$ Å, $\Lambda_2 = 38$ Å, with $\Gamma = \frac{d_{Ti}}{\Lambda} = 0.42$ and $N = 20$ for both of the two parts. This sample was designed to give two nicely distinguished sets of Bragg peaks to be used for rate calibration, see Sec. 6.1.1 and 6.1.2.

- A stack of eight multilayers with periods ranging from $15 - 120$ Å, $\Gamma = 0.46$ and a total thickness of roughly 1200 Å for each multilayer was created. The sample was deposited to be examined with transmission electron microscopy (TEM) to give insight in possibly accumulated roughness and to test the deposition system's ability to deposit very thin layers. In the layers with $d_i < 10$ Å the thickness of the initial layer was reduced.

- A multilayer with $N = 100$, $\Lambda = 48$ Å and $\Gamma = 0.46$ was deposited. The design was inspired by simulations which showed that this value for the period corresponds to the thinnest layer in an $m = 6$ supermirror.

5.2 Samples Deposited in Linköping

The main goal of these samples was to find ideal parameters to deposit high-quality multilayers. For this the effects of high-flux ion assistance, modulated ion-

assistance and different values for the substrate bias voltage on the multilayer quality were examined. All samples were grown using $\sim$ 70 W for the target powers of Co and Ti. During the time of these depositions it was not possible to create any samples containing $^{11}B_4C$ with this deposition system, see Sec. 4.

- Series 1: 4 samples using continuous high-flux ion-assistance with bias voltages varying from floating (~ -23 V) to -50 V.
- Series 2: 3 samples using modulated high-flux ion-assistance where the 3 Å thick initial layer for both materials was grown with the bias at floating potential and the bias for the final layer was varied from -30 to -50 V.

For the two series the multilayer parameters corresponded to $\Lambda = 48$ Å, $\Gamma = 0.46$ and $N = 50$. The series differ only in the used form of ion-assistance and for the samples in each of the individual series the substrate bias was varied to examine its effect on the interface roughness.

In addition to these two sets, multilayers were grown with the following parameters:

- A multilayer with $N = 100$, $\Lambda = 48$ Å and $\Gamma = 0.46$ to mimic the design of the last sample that was deposited in Hamburg with the differences being that no $^{11}B_4C$ was co-sputtered this time, high-flux ion-assistance was utilized and, therefore, smaller absolute values for the substrate bias voltage were used.
- One sample that has the same parameters as the ones of the first series but with low-flux ion-assistance and a bias of -30 V.

6 Multilayer Characterization

The characterization of the deposited multilayers was a key task of the project. Several different characterization techniques have been used to gain as much information as possible about the deposited neutron mirrors. An overview of the deployed techniques is given in this chapter.

6.1 X-ray Reflectivity

X-ray reflectivity (XRR) is a fast and versatile tool that is widely used in research to analyze thin films and multilayers. Several multilayer parameters such as the multilayer period or the thicknesses of the individual layers can be obtained. Furthermore, information about the interface width can be extracted. During XRR x-rays with a known wavelength are incident onto the sample from different grazing incident angles and the reflected beam is detected.

The reflection of x-rays from a multilayer follows the same law as neutrons which was given in (4). For the sake of completeness it is given here once again

$$m\lambda = 2\Lambda \sin\theta \sqrt{1 + \frac{\bar{n}^2 - 1}{\sin^2\theta}}.$$

Since the interfaces of the multilayer are not ideally flat in addition to the specularly scattered part of the beam there is also a part that is scattered non-specularly, i.e. diffuse, see Fig. 16. This diffuse scattering is strongly related to the interface roughness.

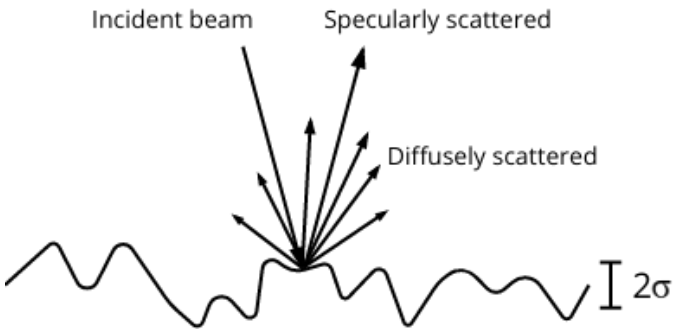

Figure 16: Illustration of an x-ray beam being scattered by a rough surface.

For the measurements in this work a powder diffractometer in Bragg-Brentano geometry was used, see Fig. 17. It has a line-focused copper anode source, operating at 1.8 kW. To attenuate the K_β-radiation a Ni β-filter was used to make sure only the K_α-radiation at $\lambda = 1.54$ Å was irradiating the sample. Measurements were performed using a 1/32° divergence slit and a 1/32° anti-scatter slit on the primary optics side to collimate the beam and limit the x-ray spot size on the sample. As

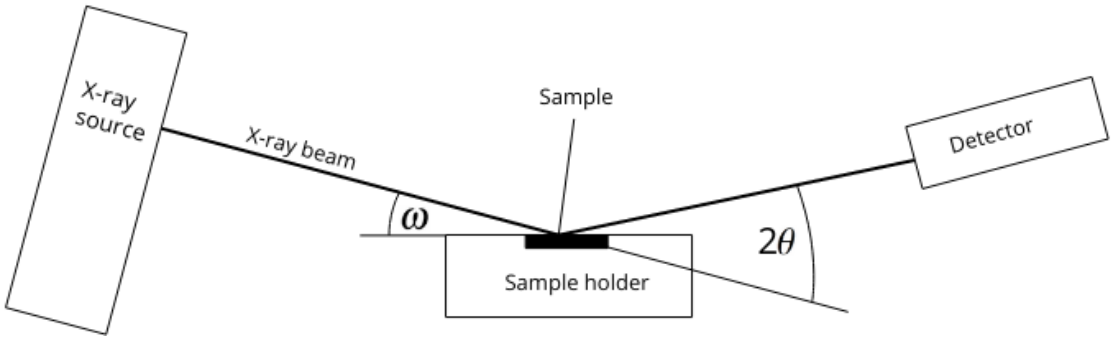

Figure 17: Illustration of the used diffractometer, for simplicity the optical devices such as slits, masks and monochromator are omitted in the picture.

secondary optics a 0.1 mm antiscatter slit was used before the reflected x-rays were detected by an X'Celerator detector.

The x-ray tube and the detector can both be rotated around the goniometer center with the rotation angles ω and $(2\theta - \omega)$, respectively. In this diffractometer the two angles are decoupled enabling both $\omega - 2\theta$ scans and rocking-curve scans.

During $\omega - 2\theta$ scans the x-ray tube and the detector are rotated simultaneously making sure that $\omega = \theta$. This means that only the specularly scattered beam is detected. During rocking-curve scans the 2θ is held constant, and only ω is varied around a the starting value $\omega = \theta$ to measure the non-specularly scattered parts which holds information about the interface roughness.

6.1.1 Calculating the Multilayer Period Λ

The multilayer period can be calculated from Bragg peak positions in the measured x-ray reflectivity data. After the scan the Bragg peaks have to be identified which delivers a discrete set of values for $m = m(\sin\theta)$ in Eq. (4) which is easily transformed to a linearized form

$$m^2 = 4\frac{\Lambda^2}{\lambda^2}\left[\sin^2\theta + \left(\bar{n}^2 - 1\right)\right] \tag{12}$$

After fitting a linear function of the form $f(x) = kx + d$ to the data points by identifying $f = m^2$ and $x = \sin^2\theta$, and $k = 4\frac{\Lambda^2}{\lambda^2}$. The slope of the fitting function determines Λ, see Fig 18.

A rough estimation for the multilayer period can be obtained by applying Bragg's law and extracting Λ. This can be useful to get a first impression already during the XRR measurement or when only one Bragg peak is visible.

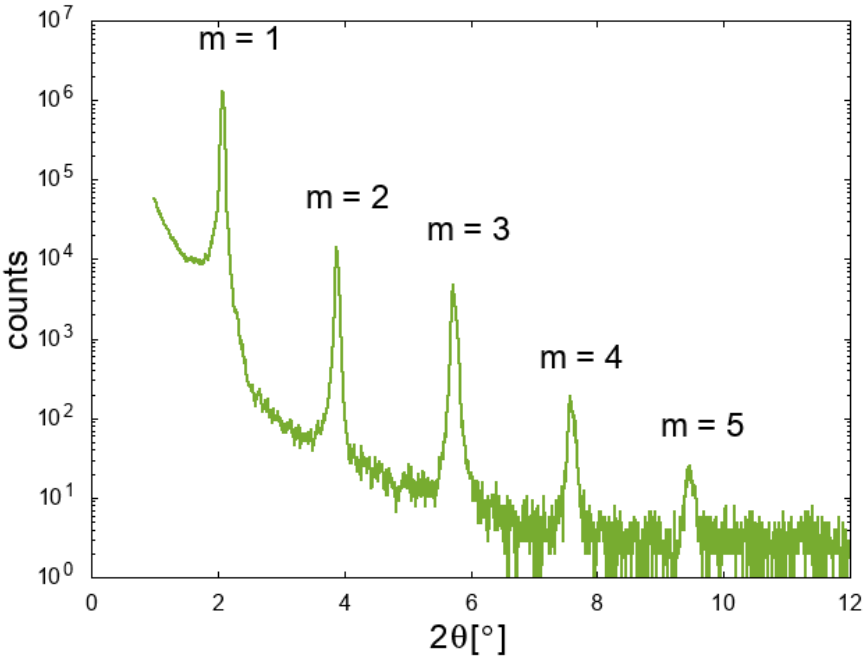

(a) X-ray reflectivity scan

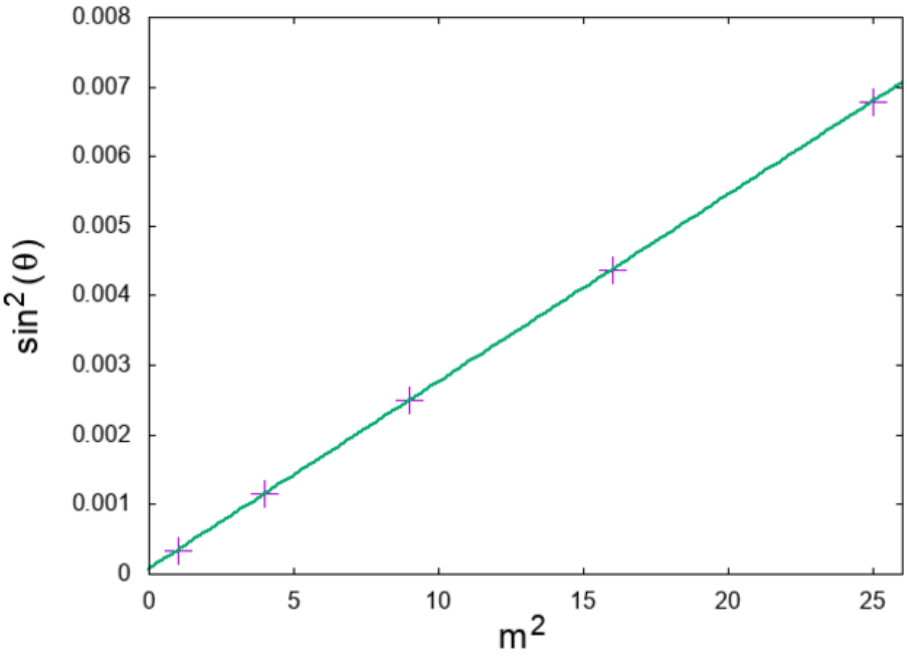

(b) Linear fit to the obtained data

Figure 18: (a) The XRR scan of a Ni-Ti multilayer. The visible five Bragg peaks are used to calculate the multilayer period Λ*. (b) Linear fit to the discrete* $\sin^2\theta$ *versus* m^2 *values. From the slope of the fit* Λ *can be extracted. In this case the aimed value was* $\Lambda_{aim} = 48.0$ Å*, the fit gave a value of* $\Lambda_{fit} = 47.1 \pm 0.14$ Å*.*

6.1.2 Determining the Growth Rates r_M

To create multilayers with the correct thicknesses of the individual layers an exact knowledge of the growth rate r_M, i.e. how many Å/s the layer grows during depo-

sition, for both materials $M = A, B$ is vital. The growth rates can be calculated via creating two periodic multilayers $i = 1, 2$ with different deposition times t_{Mi} for the two materials. After determining Λ_i for both multilayers as described in section 6.1.1 a set of linearly independent equations is obtained

$$\Lambda_i = t_{Ai} r_A + t_{Bi} r_B, \tag{13}$$

from which r_M for both materials can be easily extracted.

By depositing a stacked multilayer consisting of two parts which correspond to the two samples in the first method it is possible to get r_M from only one deposition. One only has to carefully distinguish which Bragg peak in the XRR plot comes from which part in the stack.

6.1.3 Rocking Curves

As mentioned above the same setup can be used to examine the roughness of the multilayer interfaces. This can be achieved by fixing the angles of the detector (θ) and the sample (ω) at values that correspond to one, in most cases the first order, of the Bragg peaks and then varying ω.

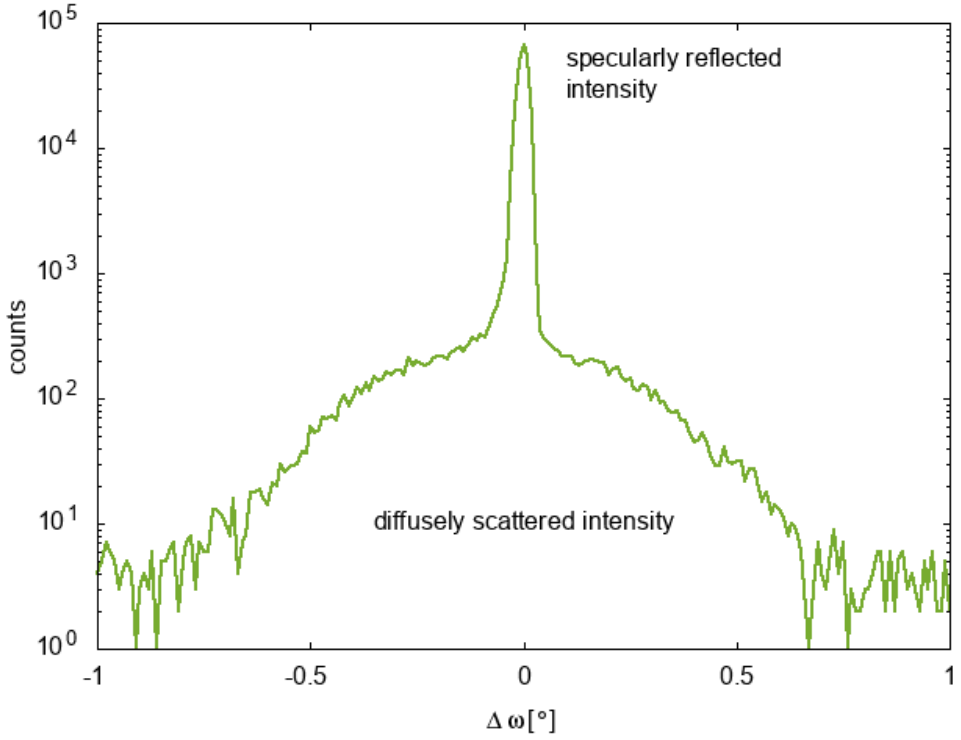

Figure 19: Rocking curve for a Co-Ti multilayer consisting of 100 bilayers, note the logarithmic scale for the intensity axis.

If the surface was perfectly flat the beam would be scattered only specularly leading to a sharp peak in the rocking curve with zero diffuse intensity. The amount

of the diffuse intensity during rocking scans was used to qualitatively compare the quality of the interfaces of the different multilayers, see Fig. 19 for an example of a diffuse reflectivity curve.

6.2 X-ray Diffraction

X-ray diffraction (XRD) is conceptually similar to XRR, probing higher values of θ in conventional θ-2θ scans. The x-ray beam is incident onto the sample and is diffracted from ordered structures, such as crystallites, that might be present in the layers.

By scanning the sample through a range of 2θ angles all possible diffraction directions of crystallites in the multilayer should be attained. From the diffracted intensity at different angles, information about the structure of the sample can be extracted.

For XRD the same diffractometer was used as for XRR, see Sec. 6.1. The only difference was that for diffraction the divergence and anti-scatter slit at the incident beam path $1/2^\circ$ slits were used.

In this work XRD was used to check if specific multilayers had amorphous structure or if crystallites had formed during growth which would lead to peaks in the XRD scan.

6.3 Transmission Electron Microscopy

Transmission electron microscopy (TEM) provides insight into the structure of the individual layers and also delivers information about the interface roughness, especially accumulated roughness when hundreds of interfaces are involved.

For this work a FEI Tecnai G2 TF 20 UT field-emission instrument operated at 200 kV was used to acquire EM images. The instrument offers a point resolution of 0.19 nm.

6.3.1 Sample Preparation

To prepare the cross sectional samples two pieces of size 1×1.8 mm^2 were cut out of the sample and placed in a titanium grid with the multilayers facing each other, see Fig. 20.

Afterwards, the sample was grinded by hand with diamond papers with increasing fineness from both sides to a thickness of about 50 μm. To make the samples electron transparent low-angle ion milling was thereafter applied.

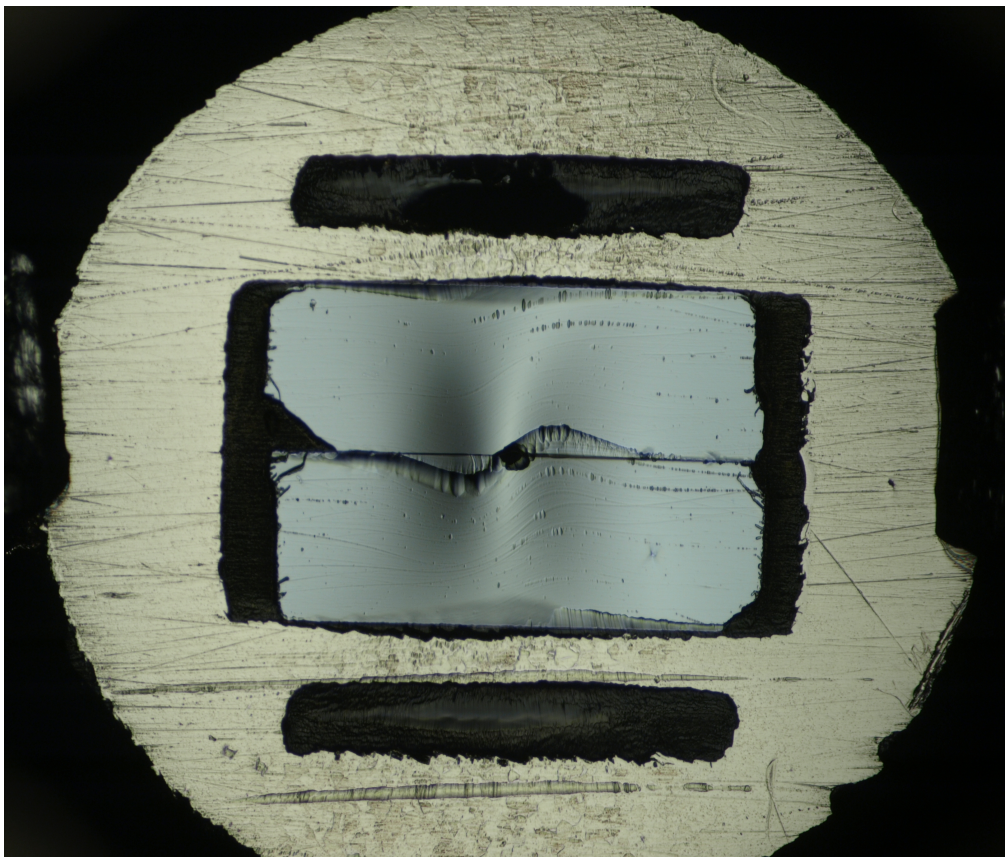

Figure 20: Polished sample mounted in the Ti grid after the ion milling and ready for transmission electron microscopy.

To remove the amorphous surface layers that may have formed in the previous step and to clean the surface a final polishing stage using low-energy ions was utilized.

6.3.2 Modes

TEM can be carried out using a variety of different imaging modes. The two most commonly used are bright field (BF) and dark field (DF) mode. The difference is that in BF mode the transmitted beam of the electrons is chosen while the DF mode detects a scattered part of the electron beam.

The contrast mechanism in both modes is very different. When the central tranmitted beam is included, i.e. BF mode, the image formation is due to mass-absorption and diffraction contrasts generated by interference of transmitted electrons. Heavier regions in the sample scatter electrons at larger angles which means they are blocked in BF mode. As a result, heavier regions appear darker in BF images because of the lower intensity of electrons and vice versa. This way the different layers of the multilayers can be depicted and interface roughness can be examined.

In DF TEM imaging mode on the other hand, the contrast is primarily caused by diffraction. This contrast arises from Bragg scattering from crystalline parts of the sample. By tilting the sample the desired Bragg reflections can be selected. This way DF imaging can be used to search for crystalline parts in a multilayer or to verify if a sample is amorphous.

In addition to that high resolution transmission electron microscopy (HRTEM) and selected area electron diffraction (SAED) were also applied.

6.4 Neutron Reflectivity

Neutron reflectivity is the most expensive characterization method used during this work. Nevertheless one sample could be sent to the Institut Laue-Langevin in Grenoble to be measured. Since the multilayers in this work are designed to be neutron mirrors neutron reflectometry represents the ultimate test for the created samples.

The principle is the same as in x-ray reflectivity, see Sec. 6.1 and how a multilayer reflects a neutron beam is described in detail in Sec. 2, which is the reason why in this chapter a description is omitted and neutron reflectivity is only mentioned for the sake of completeness.

7 Results

The created multilayers, see Sec. 5, were characterized using the techniques described in Sec. 6. The measurements gave interesting results which are presented and discussed in this chapter.

7.1 The Effect of $^{11}B_4C$

In this section the stacked multilayer and the second sample that was deposited while co-sputtering $^{11}B_4C$ are compared to the sample with $N = 100$ without any $^{11}B_4C$ but with high-flux ion-assistance. Using these three samples the effects of adding $^{11}B_4C$ on structure and quality of the multilayers were examined.

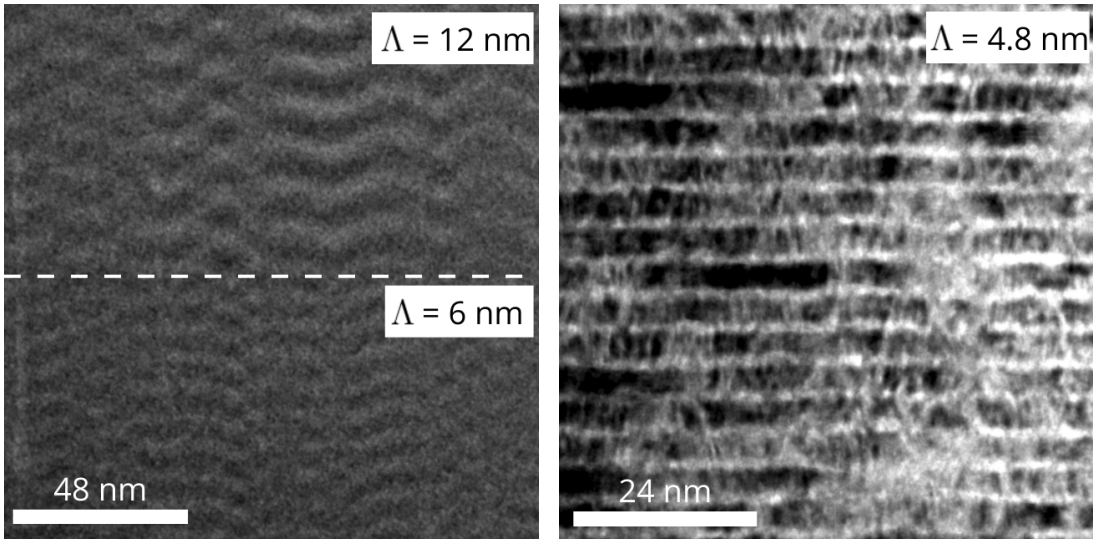

(a) amorphous Co/Ti with $^{11}B_4C$ (b) crystalline Co/Ti without $^{11}B_4C$

Figure 21: Bright field electron microscopy images to show the effect of $^{11}B_4C$. The multilayers have a period thickness of (a) $\Lambda_1 = 120$ Å (top) and $\Lambda_2 = 60$ Å (bottom) and (b) $\Lambda = 48$ Å.

Fig. 21 shows the transmission electron microscopy images of two samples, the dark and light areas are the Co and Ti layers, respectively. Fig. 21a shows the sample grown with $^{11}B_4C$, two of the multilayers in the stack can be seen. The nominal multilayer periods are $\Lambda = 120$ Å and $\Lambda = 60$ Å. It has a high degree of amorphization but the layers exhibit a wave-like structure and show a high degree of roughness.

Fig. 21b shows the multilayer grown without $^{11}B_4C$. Striking are the many crystallites that did not show up in the other sample. Peculiar is the fact that the Co layers seem to be significantly thicker than the Ti layers. The reason for this might be strong intermixing or the growth rates were determined incorrectly.

The layers in the sample without $^{11}B_4C$ exhibit a better "parallel" structure compared to the first sample. This is believed to stem from the high-flux ion-assistance which increases the surface mobility of the adsorbed atoms and improves the long-distance layer flatness.

In the high resolution transmission electron microscopy (HRTEM) image, Fig. 22a, the impression that co-sputtering $^{11}B_4C$ generates multilayers with amorphous structure is confirmed. The crystalline regions in the sample without $^{11}B_4C$, Fig. 22b show a high degree of order even ranging over several layers of the different materials.

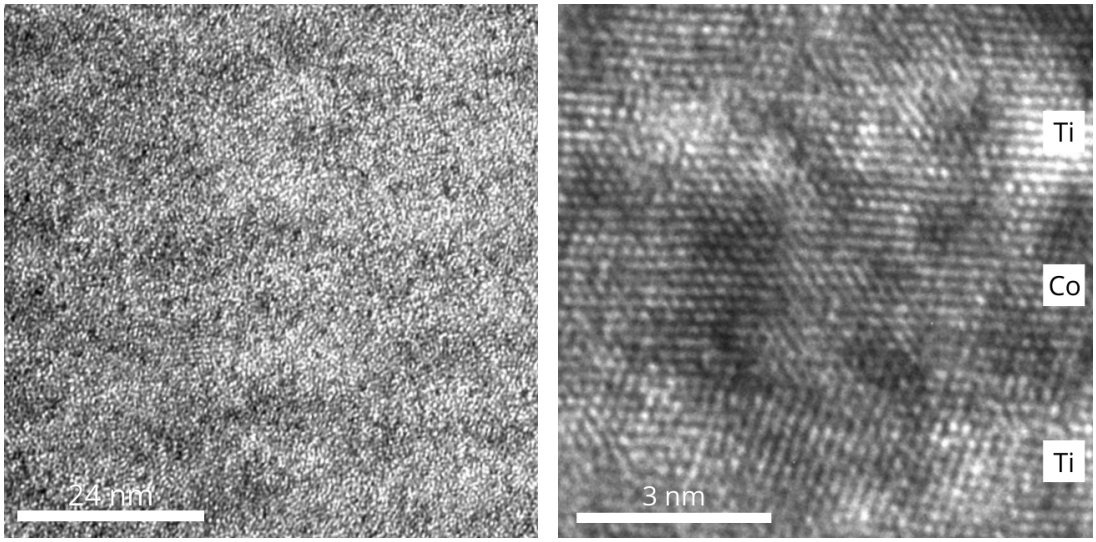

(a) amorphous Co/Ti with $^{11}B_4C$ (b) crystalline Co/Ti without $^{11}B_4C$

Figure 22: HRTEM pictures to compare the degree of order in the multilayers.

Selected area electron diffraction (SAED) was used to further confirm the amorphous and crystalline structure in the samples with and without $^{11}B_4C$, respectively, see Fig. 23. In the case of the sample grown with $^{11}B_4C$, Fig. 23a, the characteristic rings indicate electron amorphous structures while the sample without $^{11}B_4C$ gives rise to a pattern of higher intensity dots which originate from the diffraction of electrons of crystallites in the sample.

The observation that $^{11}B_4C$ hinders the formation of crystallites in the multilayers was further proven by x-ray diffraction, see Fig. 24. The absence of any diffraction peaks besides the substrate peak in the x-ray diffraction scan of the sample containing $^{11}B_4C$ (green) is another proof that no crystallites formed. In multilayers where no $^{11}B_4C$ was added peaks from the different crystalline structures emerge in the XRD data (red).

The peaks at $2\theta = 44.2°$ and at $97.7°$ in the red curve emerge from Co(111) and Co(222), respectively, while the small hump at $2\theta = 40.2°$ arises from Ti(101).

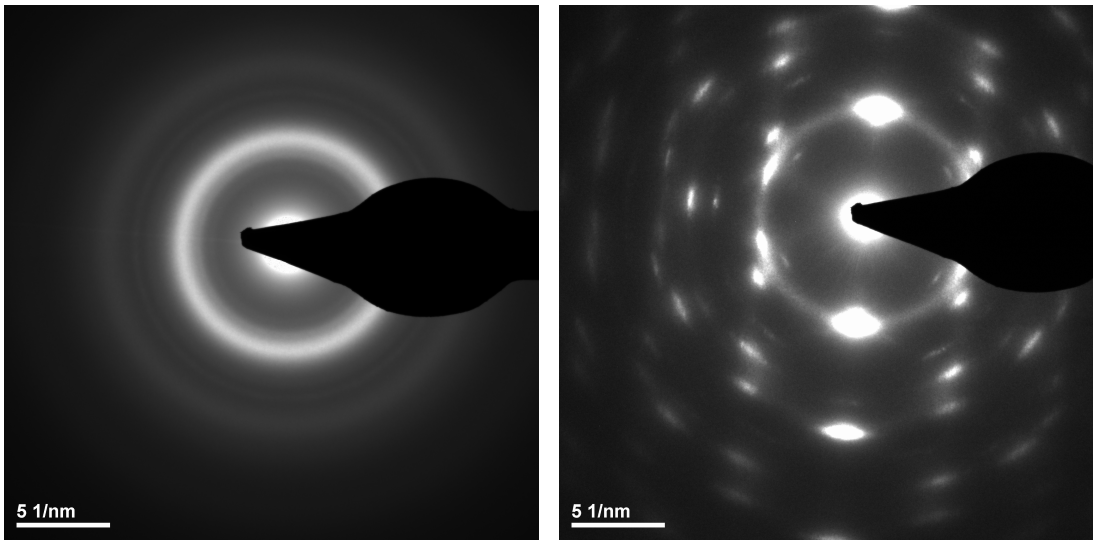

(a) amorphous Co/Ti with $^{11}B_4C$ (b) crystalline Co/Ti without $^{11}B_4C$

Figure 23: SAED images show (a) the amorphous structure in samples grown with $^{11}B_4C$ and (b) the crystalline structure in the sample without $^{11}B_4C$.

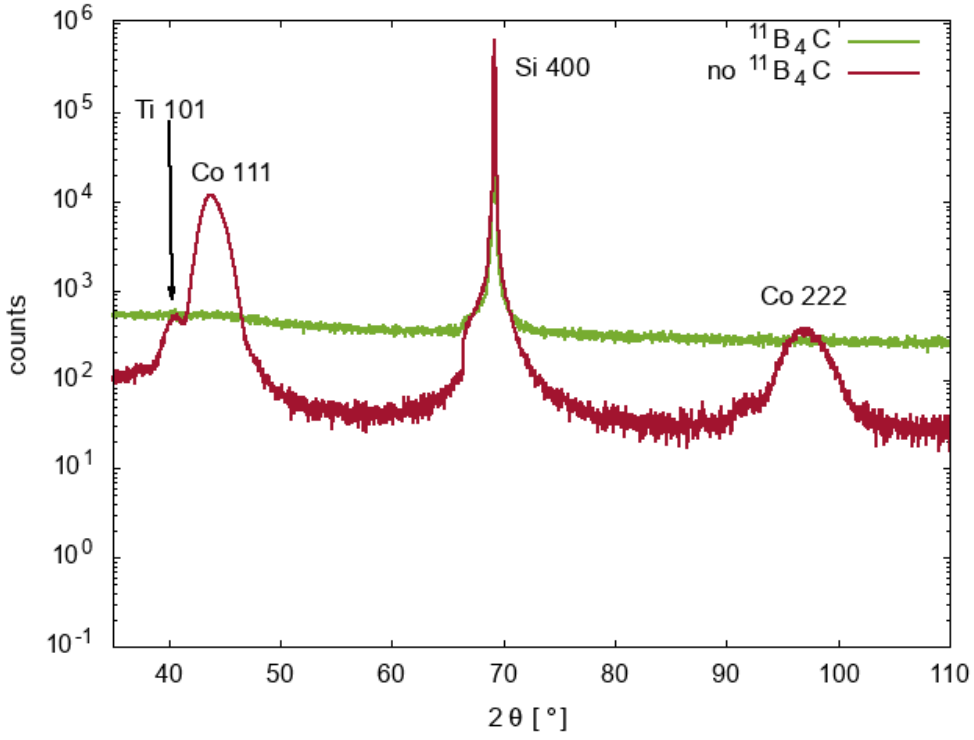

Figure 24: X-ray diffraction of Co-Ti multilayers with co-sputtered $^{11}B_4C$ (green) and without adding $^{11}B_4C$ (red).

The peak at $2\theta = 69.8°$ in both curves is the peak of the Si(100) substrate.

To examine the effect of $^{11}B_4C$ even further x-ray reflectivity measurements were performed, the reflectivity curves are shown in Fig. 25. It is obvious that the sample with $^{11}B_4C$ has sharper and stronger pronounced Bragg peaks which hints to a better overall multilayer quality.

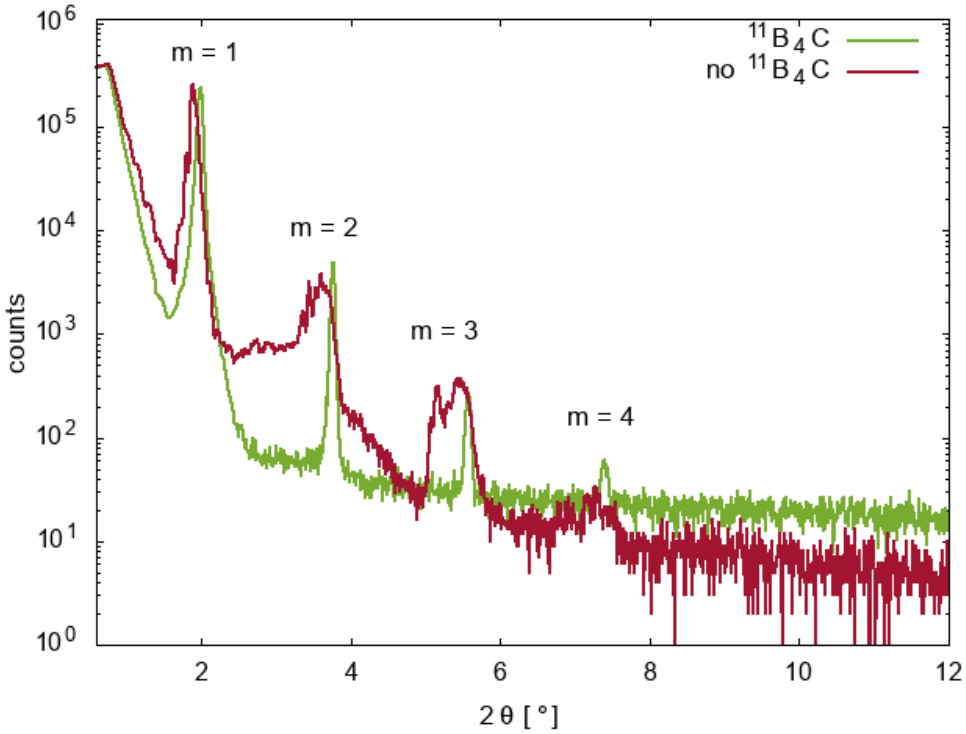

Figure 25: X-ray reflectivity measurements of two samples where one was grown with (green) and one without $^{11}B_4C$ (red).

When comparing the rocking curves at the first Bragg peak of both samples, see Fig. 26, the sample including $^{11}B_4C$ shows more diffusively scattered intensity which is an indicator of higher roughness as was already seen in the TEM pictures.

It is believed that by optimizing the growth parameters for the samples grown with $^{11}B_4C$, like ion energy, thickness of the initial layer and applying high-flux ion-assistance, the interface roughness and the "waviness" can be reduced drastically.

The crystalline phases where further examined by electron microscopy using the dark field mode. The images do not deliver any new knowledge and are therefore not shown here. However, the dark field analysis confirms the results mentioned above.

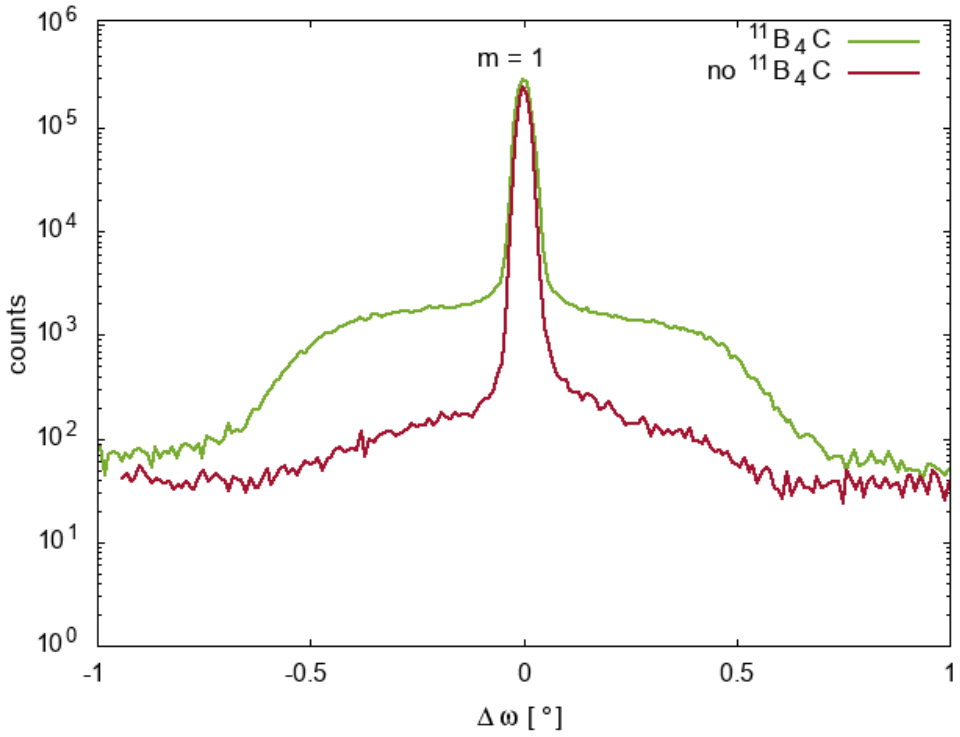

Figure 26: Rocking curves to examine the effect of $^{11}B_4C$ on the interface roughness.

7.2 Continuous Ion-assistance

Using the first series of four samples, see Sec. 5.2, that was created with the deposition system at Linköping University the effect of the substrate bias was examined. The samples were grown using continuous ion-assistance with the substrate bias at floating potential ($\sim -23\ V$), $-30\ V$, $-40\ V$ and $-50\ V$, respectively.

The reflectivity curves of the four samples are compared in Fig. 27. It can be observed that the peaks for $m = 2$ and higher experience a broadening and eventually even the peaks split into two distinguished peaks. This indicates a thickness gradient throughout the multilayers.

The higher order Bragg peaks are distinctly stronger pronounced with a substrate bias of $-40\ V$ (yellow) and $-50\ V$ (green).

The comparison of the rocking curves at the first Bragg peak of the samples is shown in Fig. 28. The curves for floating potential (blue) and $-30\ V$ (red) are very similar because the floating potential was measured to be $-24\ V$ and $-22\ V$ for Co and Ti, respectively. A substrate bias of $-40\ V$ (yellow) and $-50\ V$ (green) lead to considerably less diffusely scattered intensity which is a proof for smoother interfaces.

It is hard to gain information about intermixing between the interfaces which attenuates the specular reflectivity since the Bragg peaks of the different multilayers are slightly shifted. However, it is known from other material systems that

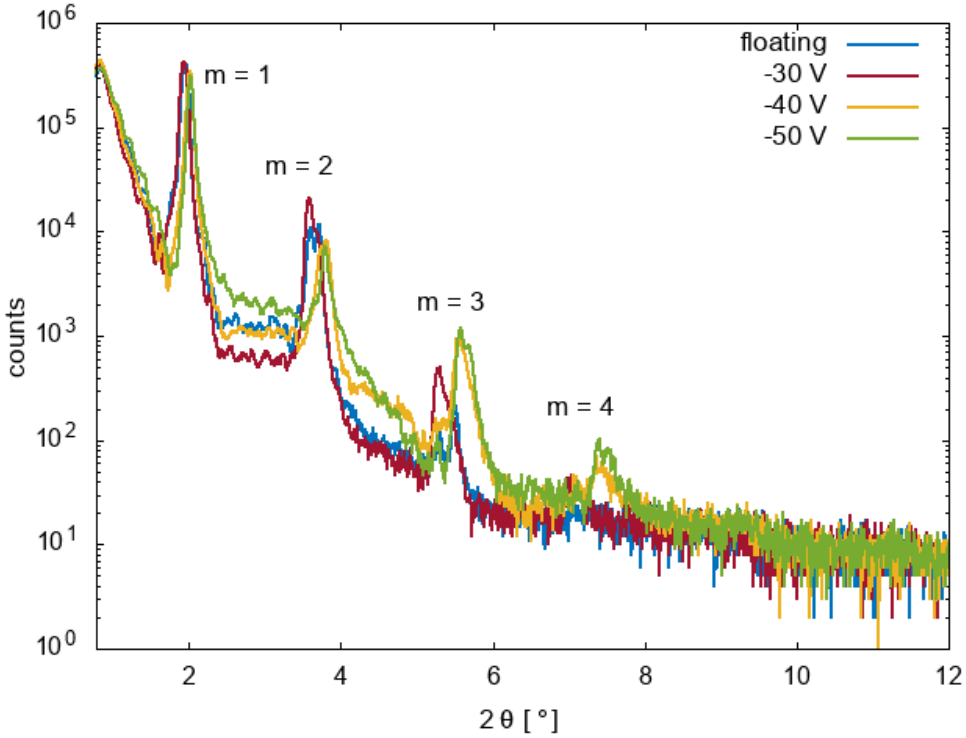

Figure 27: Reflectivity curves of multilayers grown with continuous ion-assistance with different values for the substrate bias.

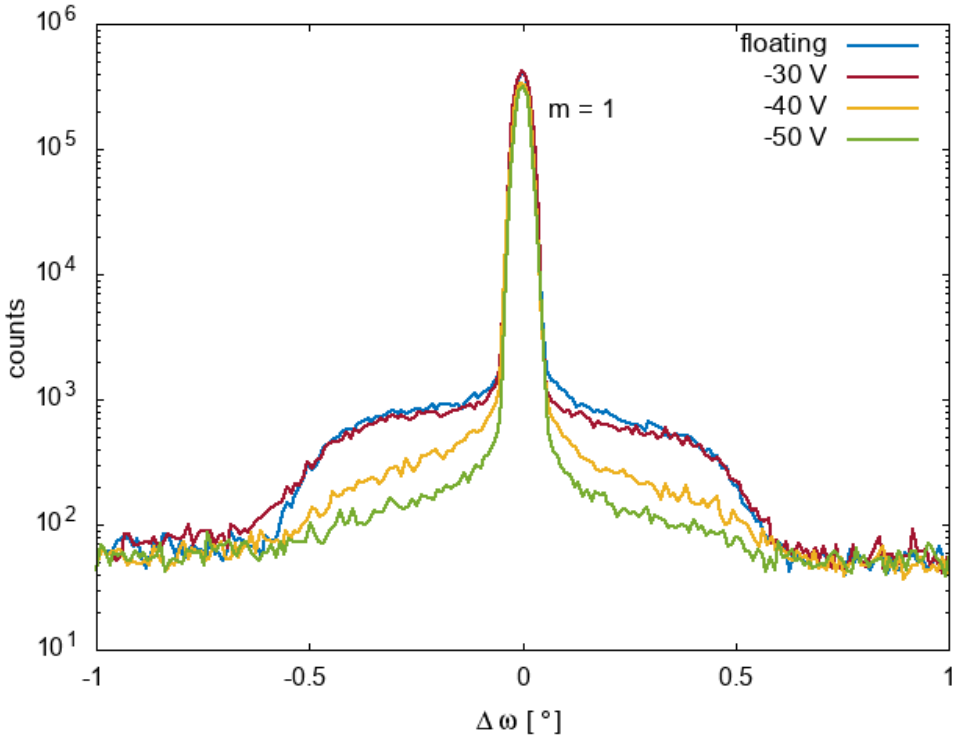

Figure 28: Rocking curves of the samples grown with continuous ion-assistance with different values for the substrate bias.

ion-assistance with high ion energies increase intermixing. On the other hand since higher ion energies lead to smoother interfaces there is always a trade-off and the perfect settings have to be found for every system.

7.3 Modulated Ion-assistance

In the same way as for continuous ion-assistance the three samples grown with modulated ion-assistance using different values for the substrate bias while growing the final layer ($-30\ V$, $-40\ V$ and $-50\ V$). The 3 Å thick initial layer was grown with the substrate being at floating potential for each sample.

As in the case of continuous ion-assistance the peaks in the XRR measurement, see Fig. 29, undergo a broadening with increasing values for m and the splitting of the Bragg peaks occurs in all three samples. With higher values for the substrate bias ($-40\ V$, yellow and $-50\ V$, green) even the Bragg peak corresponding to $m = 5$ is slightly pronounced.

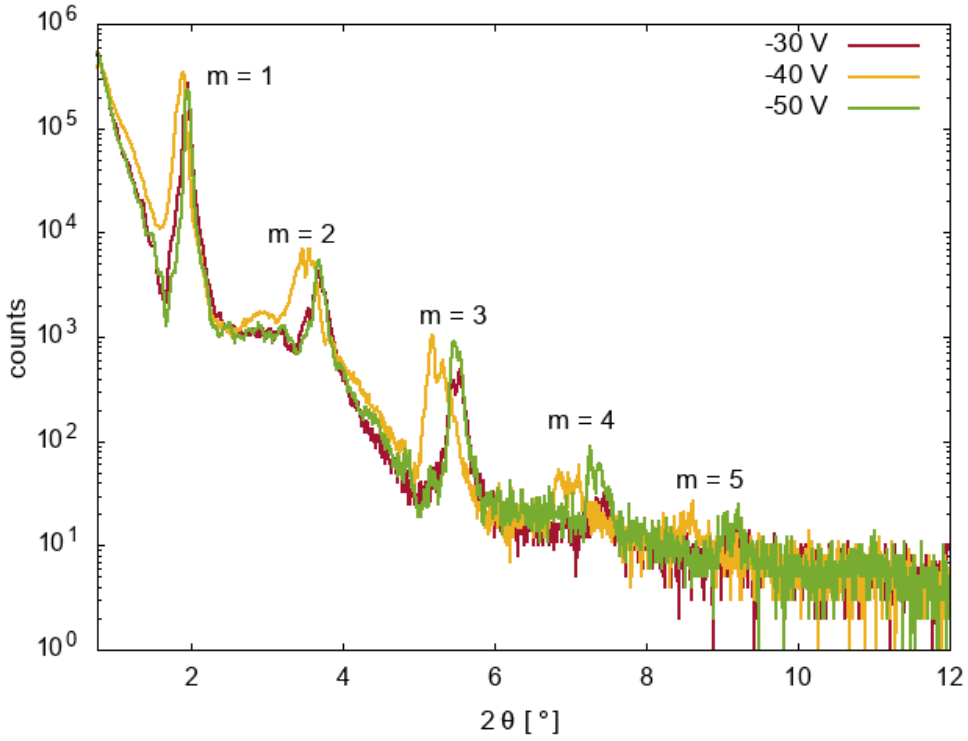

Figure 29: The reflectivity curves of the samples grown with modulated ion-assistance using different values for the substrate bias during growth of the final layer.

To compare the interface roughness qualitatively Fig. 30 shows the rocking curves of the three samples at the first Bragg peak. The diffusely scattered intensity is almost the same for all three multilayers but interestingly, in contrast to the

case of continuous ion-assistance, the sample grown with the highest ion energy (substrate bias of $-50\ V$, green) shows the most intensity for the diffusely scattered part.

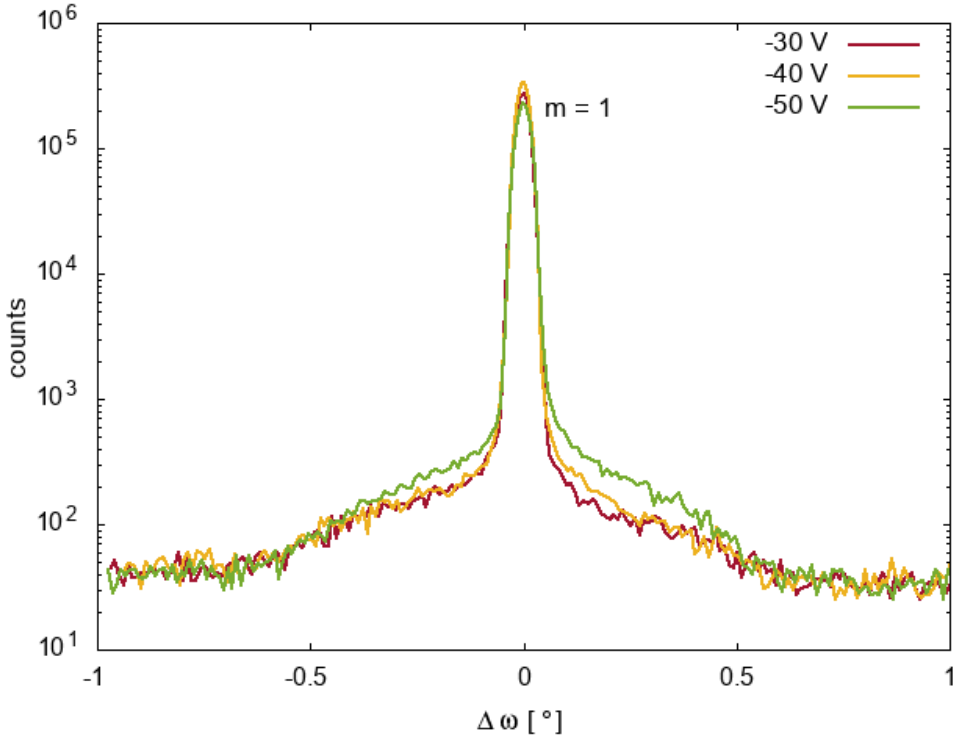

Figure 30: Comparison of the rocking curves at the first Bragg peak for three multilayers grown using modulated ion-assistance. The samples differ only in the value for the substrate bias during growth of the final layer.

These results indicate that ion energy modulation has only a weak effect when growing crystalline multilayers. As in the case for continuous ion-assistance intermixing could not be examined but again when choosing the ion energy for the ion-assistance one has to compromise between roughness and intermixing and modulating the ion-assistance could be a vital tool minimize both.

7.4 Continuous vs. Modulated Ion-assistance

Using the same samples as in the two previous sections it is possible to compare the effect of modulated ion-assistance vs. continuous ion-assistance. Fig. 31a and Fig. 31b compare the rocking curves of two samples. In each case one sample was grown using continuous ion-assistance with a substrate bias of $-30\ V$ and $-40\ V$, respectively, and the other sample used the same substrate bias but first a 3 Å thick initial layer was grown at floating potential.

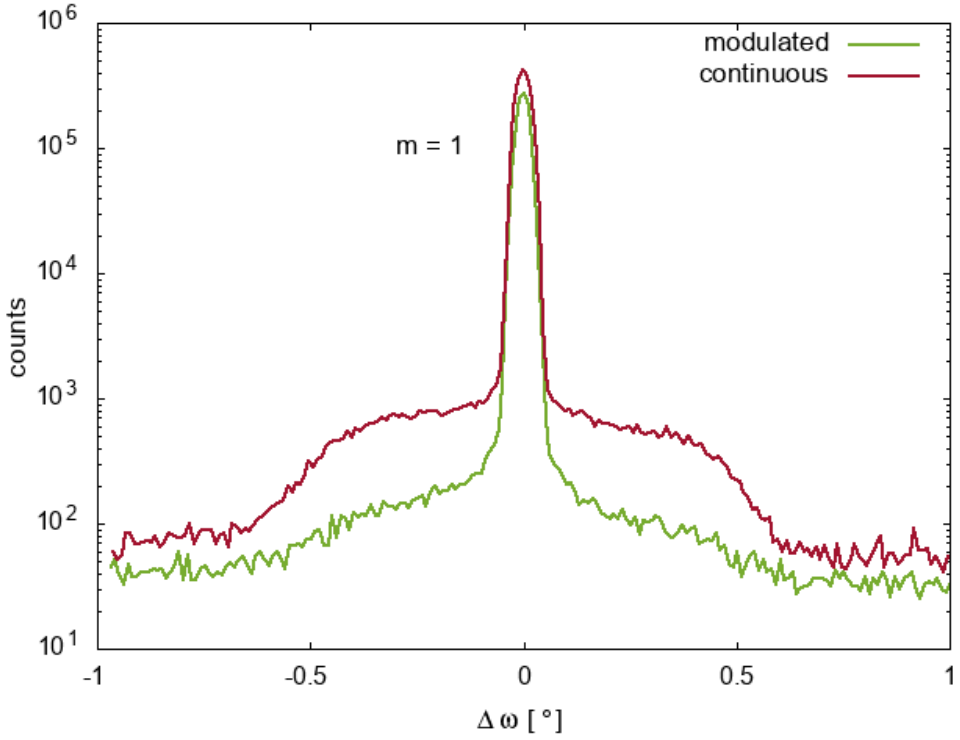

(a) substrate bias = $-30\ V$

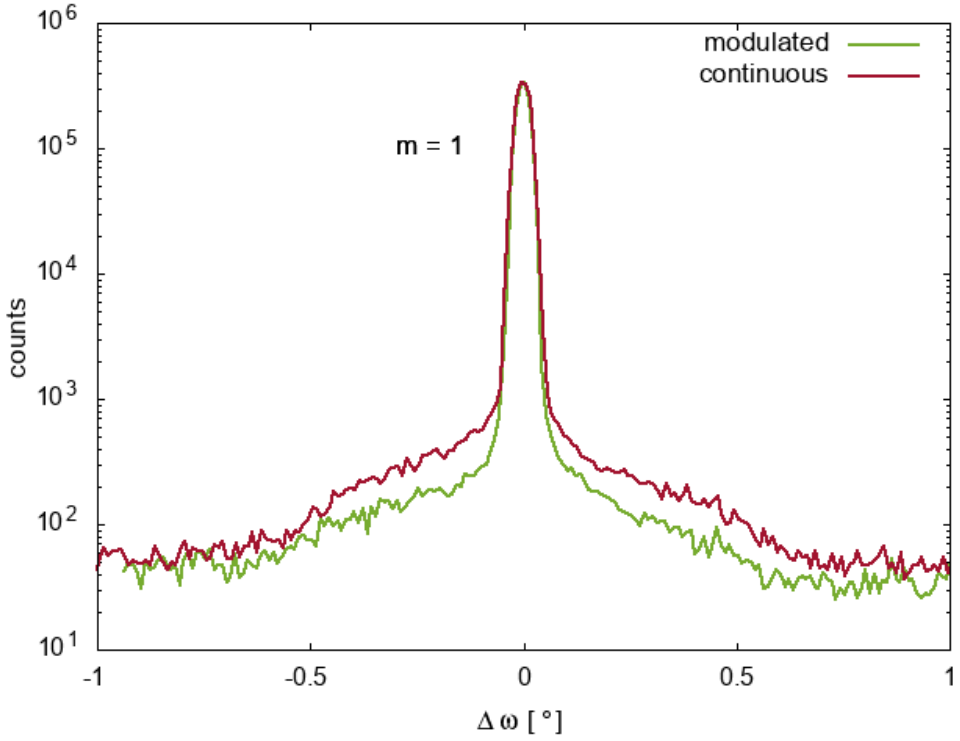

(b) substrate bias = $-40\ V$

Figure 31: X-ray reflectivity data to examine the effect ion-assistance modulation (green) vs. continuous ion-assistance (red). (a) the rocking curves at the first Bragg peak of samples grown with a substrate bias of $-30\ V$ *and (b)* $-40\ V$*.*

In both cases the rocking curves of the samples grown with modulated ion-assistance indicates less interface roughness but the difference is more pronounced for lower ion energies.

When using a substrate bias of $-50\ V$ the diffusive scattered intensity in the rocking scan for the sample grown with continuous ion-assistance is slightly less than the one with modulated ion-assistance. On the other hand the reflectivity scan, see Fig. 32, for modulated ion-assistance (green) implies that the multilayer quality with modulated ion-assistance is better since the broadening of the Bragg peaks is less pronounced and the peak corresponding to $m = 5$ is still slightly visible which is not the case for the sample grown with continuous ion-assistance (red).

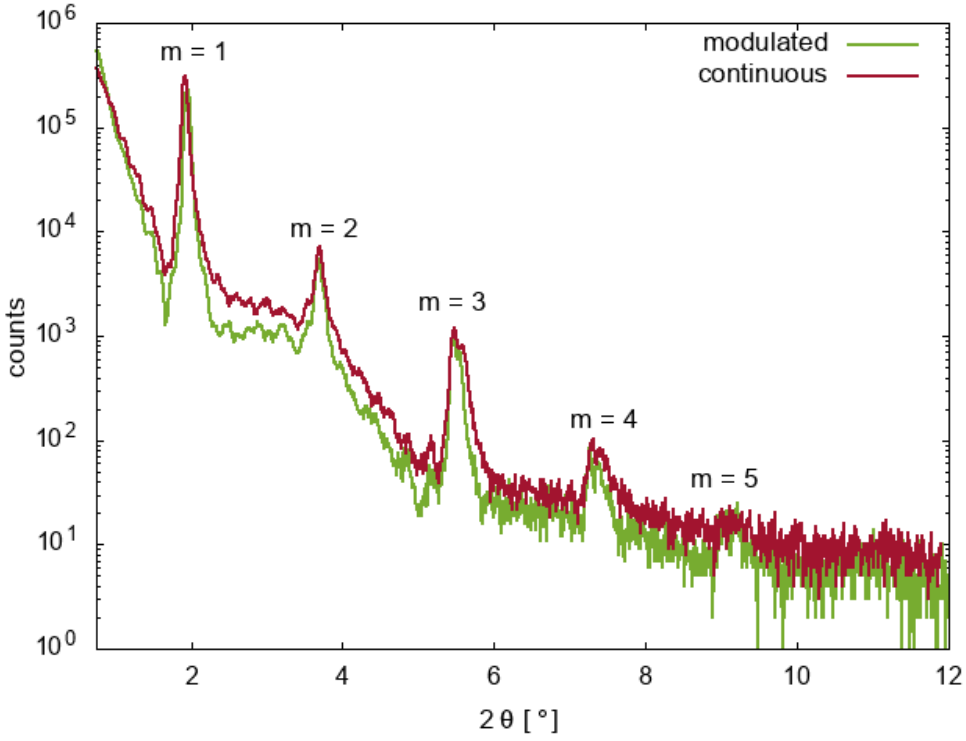

Figure 32: X-ray reflectivity measurement of samples grown with a substrate bias of $-50\ V$ once with modulated ion-assistance (green) and once with continuous ion-assistance(red).

7.5 High-flux vs. Low-flux Ion-assistance

As described in Sec. 3.2 ion-assistance can be improved by generating a higher flux of ions that hit the substrate during growth. Fig. 33 shows the data of the x-ray reflectivity measurements of two samples grown with continuous ion-assistance. The only difference is that in one case (red) the solenoid around the substrate was turned off leading to continuous low-flux ion-assistance while the growth of

the second multilayer (green) was performed with a current of 5 A through the solenoid generating a continuous high-flux ion-assistance.

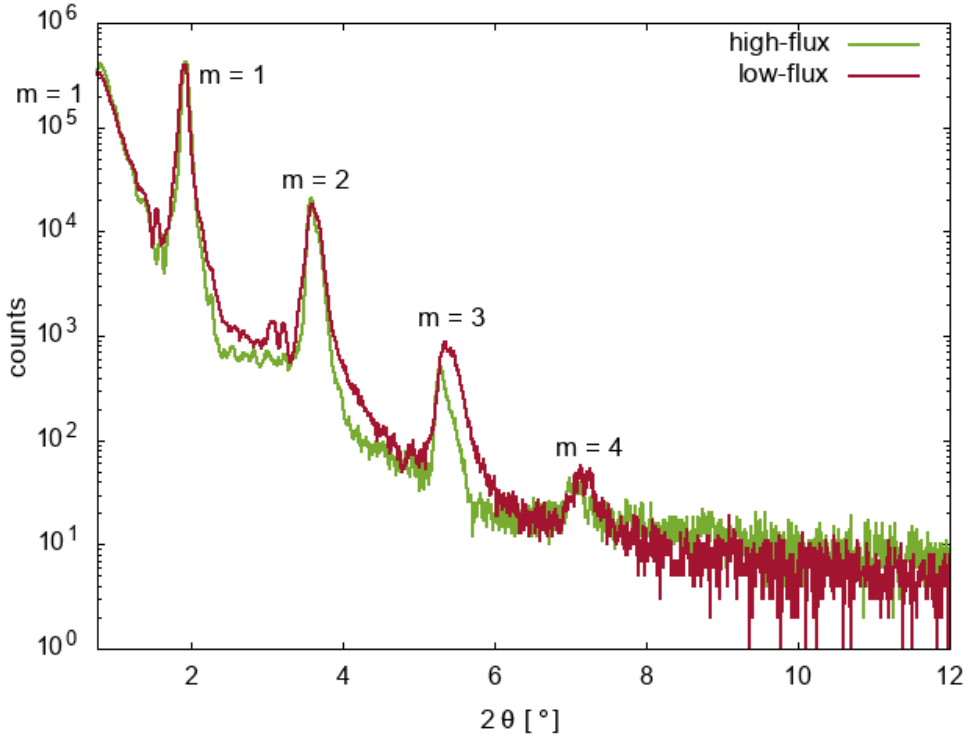

Figure 33: X-ray reflectivity of two samples one grown with high-flux (green) and one with low-flux ion-assistance (red).

The reflectivity curves have a similar shape but in the case of the multilayer grown with high-flux ion-assistance the broadening of the Bragg peaks is slightly less pronounced.

Additionally the rocking curve shows slightly less intensity in the diffusely scattered regime than in the case of low-flux ion-assistance, see Fig. 34, but the effect is very small.

Both of the observations mentioned above indicate that using high-flux ion-assistance improves the multilayer quality only a little. The effect is far weaker than was reported in [30]. The difference in the results probably rises from the fact that in that publication amorphous multilayers were examined while the samples tested in the measurements here are crystalline structures shown by the XRD measurement, see Fig. 35.

As was shown in Sec 7.1, depositing amorphous multilayers without high-flux ion-assistance leads to high roughness and not parallel interfaces. It is believed that high-flux ion-assistance can improve the quality of amorphous multilayers drastically.

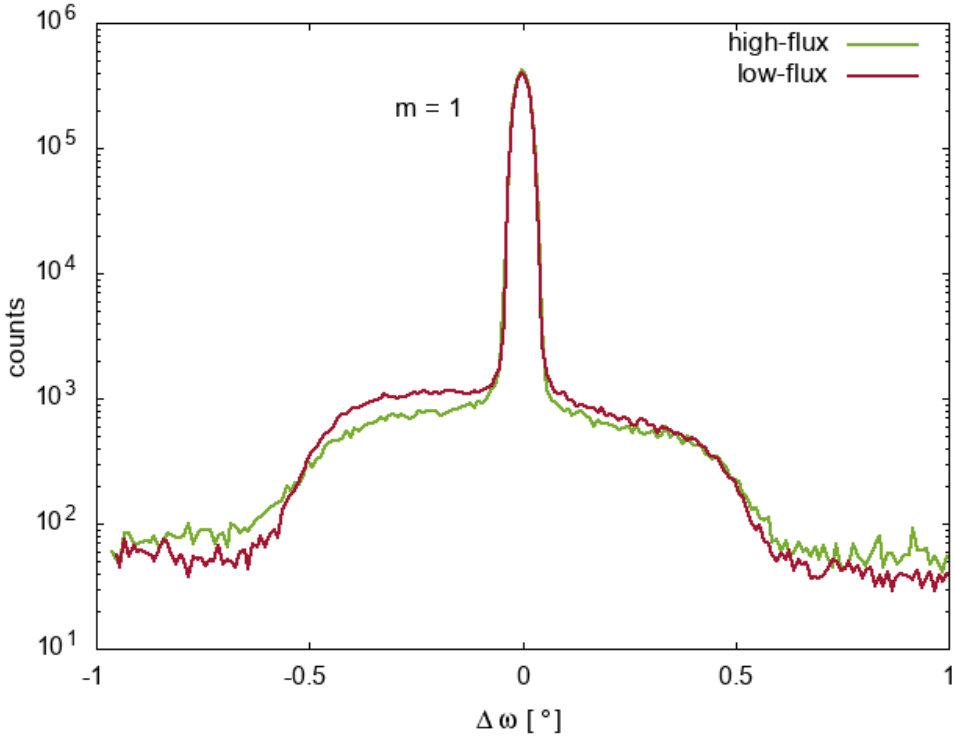

Figure 34: Rocking curves at the first Bragg peak of two samples one grown with high-flux (green) and one with low-flux ion-assistance (red).

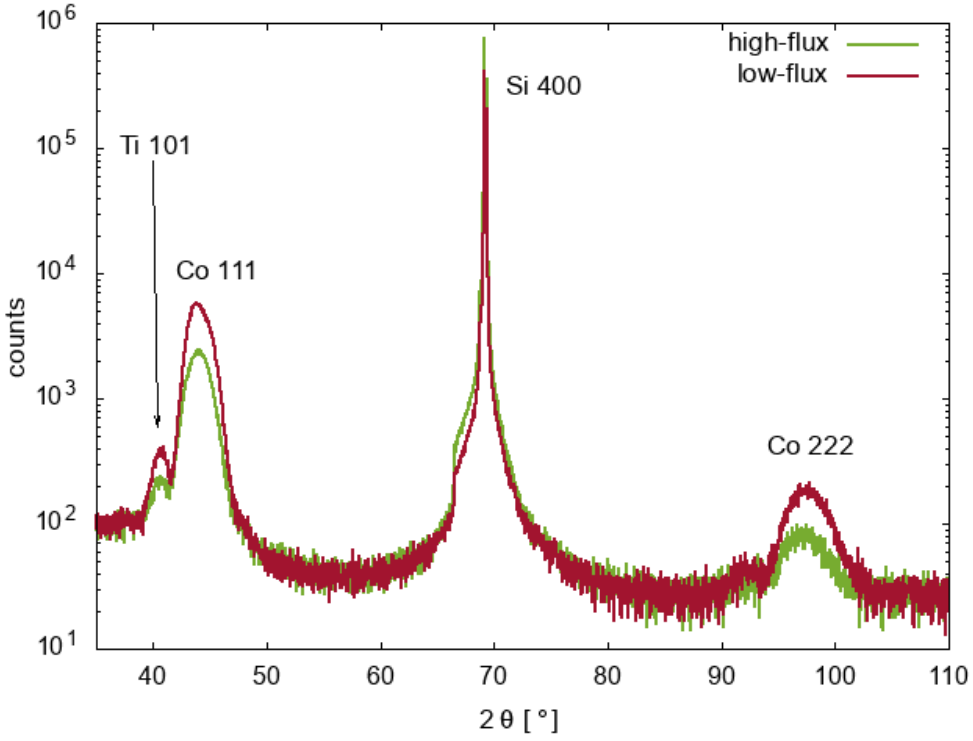

Figure 35: X-ray diffraction scan of two samples where one was grown using high-flux (green) and one using low-flux ion-assistance (red).

7.6 Neutron Reflectivity

As mentioned above the multilayer with $N = 100$, $\Lambda = 48$ Å and $\Gamma = 0.46$ which contains $^{11}B_4C$ was measured by neutron reflectivity with a wavelength of $\lambda = 5.183$ Å, see Fig. 36.

The measurements were performed in Grenoble at the neutron scattering facility Institute Laue-Langevin, ILL, using the Swedish neutron reflectometer Super-ADAM, see [38]. The detector is a 2D position sensitive 3-He detector, 30 × 30 cm^2 in size.

The neutron reflectivity measurements were conducted at room temperature and since only non-polarizing reflectivity properties were examined no specific sample environment was needed. A step size of 0.02° in 2θ was used with a counting time of 50 s / step.

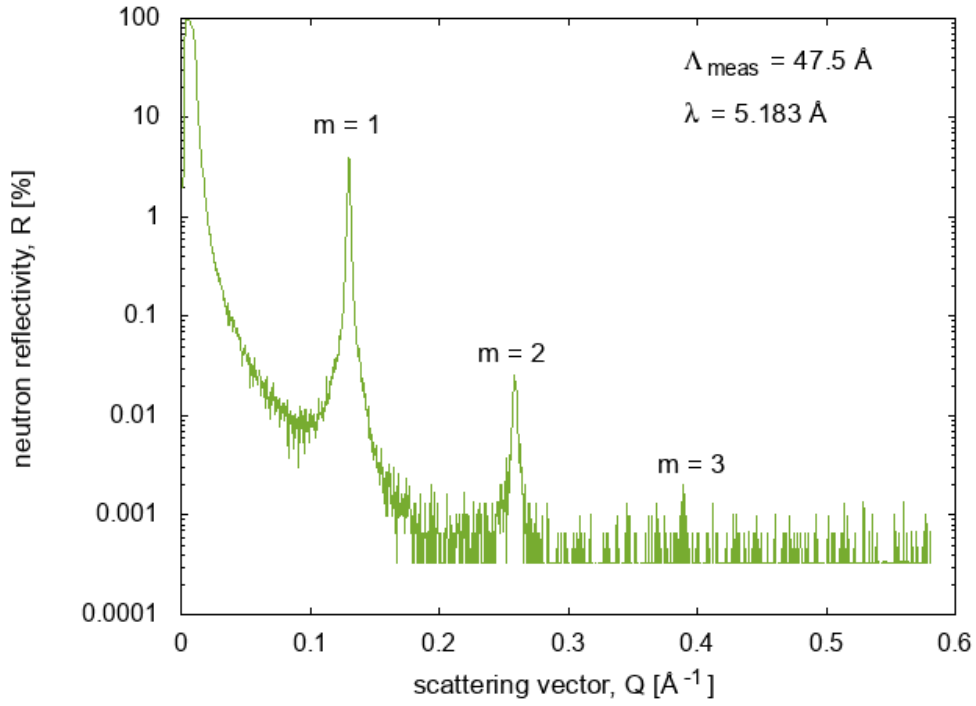

Figure 36: Neutron reflectivity scan of a sample that contains $^{11}B_4C$ grown with low-flux ion-assistance.

The absolute neutron reflectivity of the first Bragg peak is only ∼ 4% due to the high roughness that arises when depositing multilayers with low-flux ion-assistance.

Fig. 37 shows the rocking curve of the same sample. The high intensity in the diffusely scattered part confirms that the interfaces in the multilayer suffer from a high roughness.

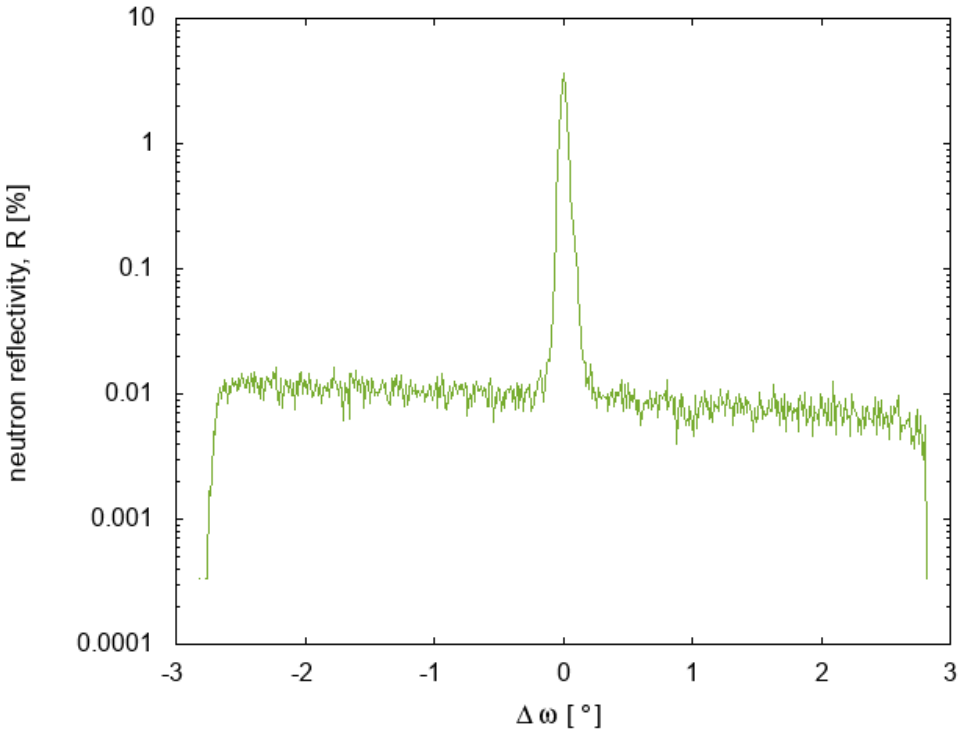

Figure 37: Diffuse neutron reflectivity measurement of the sample that was sent to Grenoble.

Regardless of the low quality in the sample the neutron reflectivity measurements show that the deposited multilayers are fully functional neutron mirrors.

8 Conclusion

Various characterization methods, including x-ray reflectivity and diffraction, transmission electron microscopy and neutron reflectivity, have been applied to a wide range of Co/Ti multilayers.

The samples were grown by direct current magnetron sputter deposition using different conditions with two different deposition systems. The goal was to find the ideal growth parameters to deposit high-quality multilayers to be used as polarizing neutron mirrors.

When Co/Ti neutron mirrors are deposited the main challenges are to reduce interface roughness, create parallel interfaces and to prevent the formation of crystallites. In this work various techniques have been tested to improve the multilayer qualitity and different ways of applying ion-assistance were examined.

The strongest influence on the multilayer quality has proven to be co-sputtering $^{11}B_4C$ continuously during multilayer growth since it prevents the formation of crystallites that causes interface roughness. Of the two deposition systems that were used only one was ready to deposit multilayers containing $^{11}B_4C$ which is the reason why further investigation of the effect of $^{11}B_4C$ was not possible during the work for this thesis.

Furthermore, by controlling the energy of the ions that bombard the sample during growth in a way that the first part of each layer is grown with low-energy ion-assistance and the second part with higher ion energy, has a positive effect on the multilayer quality. This approach of the so-called modulated ion-assistance has proven to be vital to improve the multilayer quality.

Especially when depositing amorphous layers the possibility of controlling the flux of ions that hit the sample is believed to be an important tool to deposit high-quality multilayers. Samples that were deposited using high-flux ion-assistance showed less roughness and better parallelism throughout the interfaces. During deposition of crystalline multilayers the effect was noticable as well but not as strongly pronounced.

However, to receive the best possible conditions for depositing polarizing multilayer neutron mirrors many more parameters have to be examined and, if necessary, adjusted. These include for example the thickness of the initial layer, the amount of $^{11}B_4C$ in the multilayer, the target powers, working gas pressure and the flux of the ions.

In summary, all results obtained indicate that the ideal settings to deposit high-quality polarizing multilayer neutron mirrors are co-sputtering of $^{11}B_4C$ to prevent crystallite formation, using high-flux ion-assistance to decrease roughness

and improve interface flatness and to use modulated ion-assistance to minimize both intermixing and roughness at the same time.

As a result of this thesis both of the mentioned deposition systems will be upgraded: In the deposition system in Linköping a fully functional third magnetron will be added making co-sputtering $^{11}B_4C$ possible while in the deposition system in Hamburg a solenoid will be installed to offer the possibility of controlling the flux of the ion-assistance.

References

[1] V. Pusenkov, N. Pleshanov, V. Syromyatnikov, V. Ulyanov and A. Schebetov, *New possibilities of polarised neutron reflectometry in the study of domain structure of thin magnetic films*, Physica B **234-236,** 519–521 (1997).

[2] D. Wiesler and C. Majkrzak, *Neutron reflectometry studies of surface oxidation*, Physica B **198,** 181–186 (1994).

[3] J. W. Kiel, M. E. Mackay, B. J. Kirby, B. B. Maranville and C. F. Majkrzak, *Phase-sensitive neutron reflectometry measurements applied in the study of photovoltaic films*, J. Chem. Phys. **133,** 074902 (2010).

[4] D. L. Windt, *IMD-Software for Modeling the Optical Properties of Multilayer Films*, Comput. Phys. **12,** 360–370 (1998).

[5] E. Fermi and L. Marshall, *Interference Phenomena of Slow Neutrons*, Phys. Rev. **71,** 666–677 (1947).

[6] R. Cubitt and G. Fragneto, *Neutron Reflection: Principles and Examples of Applications*, in R. Pike and P. Sabatier (eds.), *Scattering,* Academic Press, London (2002)

[7] M. Peshkin and G. R. Ringo, *On the Repulsion of Slow Neutrons by Attractive Potentials*, Am. J. Phys. **39,** 324–327 (1971).

[8] A. M. Saxena and B. P. Schoenborn, *Multilayer neutron monochromators*, Acta Cryst. A **33,** 805–813 (1977).

[9] F. Mezei, *Novel polarized neutron devices: supermirror and spin component amplifier*, Comm. Phys. **1,** 81–85 (1976).

[10] J. W. Lynn, J. K. Kjems, L. Passell, A. M. Saxena and B. P. Schoenborn, *Iron–germanium multilayer neutron polarizing monochromators*, J. Appl. Cryst. **9,** 454–459 (1976).

[11] P. Dhez and C. Weisbuch, *Physics, fabrication, and applications of multilayered structures / edited by P. Dhez and C. Weisbuch,* Plenum Press New York (1988)

[12] M. Hino, M. Kitaguchi, H. Hayashida, S. Tasaki, T. Ebisawa, R. Maruyama, N. Achiwa and Y. Kawabata, *A study on reflectivity limit of neutron supermirror*, Nucl. Instrum. Methods **600,** 207–209 (2009).

[13] T. Ebisawa, N. Achiwa, S. Yamada, T. Akiyoshi and S. Okamato, *Neutron Reflectivities of Ni-Mn and Ni-Ti Multilayers for Monochromators and Supermirrors*, Nucl. Sci. Tech. **16,** 647–659 (1979).

[14] O. Elsenhans, P. Böni, H. Friedli, H. Grimmer, P. Buffat, K. Leifer, J. Söchtig and I. Anderson, *Development of Ni/Ti multilayer supermirrors for neutron optics*, Thin Solid Films **246,** 110–119 (1994).

[15] K. Soyama, W. Ishiyama and K. Murakami, *Enhancement of reflectivity of multilayer neutron mirrors by ion polishing: optimization of the ion beam parameters*, J. Phys. Chem. Solids **60,** 1587–1590 (1999).

[16] M. Hino, H. Sunohara, Y. Yoshimura, R. Maruyama, S. Tasaki, H. Yoshino and Y. Kawabata, *Recent development of multilayer neutron mirror at KURRI*, Nucl. Instrum. Methods **529,** 54–58 (2004).

[17] R. Maruyama, D. Yamazaki, T. Ebisawa, M. Hino and K. Soyama, *Development of neutron supermirror with large-scale ion-beam sputtering instrument*, Physica B **385-386,** 1256–1258 (2006).

[18] Z. Zhang, Z.-S. Wang, J.-T. Zhu, Y.-R. Wu, B.-Z. Mu, F.-L. Wang, S.-J. Qin and L.-Y. Chen, *Design, Fabrication and Measurement of Ni/Ti Multilayer Used for Neutron Monochromator*, Chin. Phys. Lett. **24,** 3365 (2007).

[19] J. L. Wood, *Status of supermirror research at OSMC*, Proc. SPIE **1738,** 1738 (1992).

[20] R. Maruyama, D. Yamazaki, T. Ebisawa and K. Soyama, *Development of high-reflectivity neutron supermirrors using an ion beam sputtering technique*, Nucl. Instrum. Methods Phys. Res **600,** 68–70 (2009).

[21] B. P. Schoenborn, D. L. D. Caspar and O. F. Kammerer, *A novel neutron monochromator*, J. Appl. Cryst. **7,** 508–510 (1974).

[22] C. Klauser, T. Bigault, N. Rebrova and T. Soldner, *Ultra-Sensitive Depolarization Study of Polarizing CoTi Supermirrors with the Opaque Test Bench*, Phys. Procedia **42,** 99–105 (2013).

[23] T. Bigault, G. Delphin, A. Vittoz, V. Gaignon and P. Courtois, *Recent polarizing supermirror projects at the ILL*, J. Phys.: Conf. Ser. **528,** 012017 (2014).

[24] A. Biswas, R. Sampathkumar, A. Kumar, D. Bhattacharyya, N. K. Sahoo, K. D. Lagoo, R. D. Veerapur, M. Padmanabhan, R. K. Puri, D. Bhattacharya,

S. Singh and S. Basu, *Design and development of an in-line sputtering system and process development of thin film multilayer neutron supermirrors*, Rev. Sci. Instrum. **85,** 123103 (2014).

[25] A. Biswas, A. Porwal, D. Bhattacharya, C. L. Prajapat, A. Ghosh, M. Nand, C. Nayak, S. Rai, S. N. Jha, M. R. Singh, D. Bhattacharyya, S. Basu and N. K. Sahoo, *Effect of dry air on interface smoothening in reactive sputter deposited Co/Ti multilayer*, Appl. Surf. Sci. **416,** 168–177 (2017).

[26] J. Stahn and D. Clemens, *A remanent Fe/Si supermirror transmission polarizer*, Appl. Phys. A **74,** 1532–1534 (2002).

[27] D. Merkel, Z. Horváth, D. Szcs, R. Kovács-Mezei, G. Kertész and L. Bottyán, *Stress relaxation in Fe/Si neutron supermirrors by He+ irradiation*, Physica B **406,** 3238–3242 (2011).

[28] R. Maruyama, D. Yamazaki, S. Okayasu, M. Takeda, N. Zettsu, M. Nagano, K. Yamamura, H. Hayashida and K. Soyama, *Effect of Si interlayers on the magnetic and mechanical properties of Fe/Ge neutron polarizing multilayer mirrors*, J. Appl. Phys. **111,** 063904 (2012).

[29] R. Maruyama, D. Yamazaki, K. Akutsu, T. Hanashima, N. Miyata, H. Aoki, M. Takeda and K. Soyama, *Development of high-polarization Fe/Ge neutron polarizing supermirror: Possibility of fine-tuning of scattering length density in ion beam sputtering*, Nucl. Instrum. Methods **888,** 70–78 (2018).

[30] N. Ghafoor, F. Eriksson, A. Aquila, E. Gullikson, F. Schäfers, G. Greczynski and J. Birch, *Impact of B4C co-sputtering on structure and optical performance of Cr/Sc multilayer X-ray mirrors*, Opt. Express **25,** 18274–18287 (2017).

[31] C. Schanzer, M. Schneider and P. Böni, *Neutron Optics: Towards Applications for Hot Neutrons*, J. Phys.: Conf. Ser. **746,** 012024 (2016).

[32] S. Bajt, D. G. Stearns and P. A. Kearney, *Investigation of the amorphous-to-crystalline transition in Mo/Si multilayers*, J. Appl. Phys. **90,** 1017–1025 (2001).

[33] J. Colligon, *Ion–assisted sputter deposition*, Philos. Trans. Royal Soc. **362,** 103–116 (2004).

[34] N. Ghafoor, *Materials Science of Multilayer X-Ray Mirrors*, Ph.D. Thesis, Linköping Studies in Science and Technology, Sweden (2008).

[35] J. L. Schroeder, W. Thomson, B. C. Howard, N. Schell, L. Näslund, L. Rogström, M. P. Johansson-Jõesaar, N. Ghafoor, M. Odén, E. Nothnagel, A. Shepard, J. Greer and J. Birch, *Industry-relevant magnetron sputtering and cathodic arc ultra-high vacuum deposition system for in situ x-ray diffraction studies of thin film growth using high energy synchrotron radiation.*, Rev. Sci. Instrum. **86,** 095113 (2015).

[36] N. Ghafoor, F. Eriksson, P. Persson, L. Hultman and J. Birch, *Effects of ion-assisted growth on the layer definition in Cr/Sc multilayers*, Thin Solid Films **516,** 982–990 (2008).

[37] F. Eriksson, *Soft X-ray Multilayer Mirrors*, Ph.D. thesis, Linköping Studies in Science and Technology, Sweden (2004).

[38] A. Devishvili, K. Zhernenkov, A. J. C. Dennison, B. P. Toperverg, M. Wolff, B. Hjörvarsson and H. Zabel, *SuperADAM: Upgraded polarized neutron reflectometer at the Institut Laue-Langevin*, Rev. Sci. Instrum. **84,** 025112 (2013).